A review of Holocene solar-linked climatic variation on centennial to millennial timescales: Physical processes, interpretative frameworks and a new multiple cross-wavelet transform algorithm

Willie Soon [a,*], Victor M. Velasco Herrera [b], Kandasamy Selvaraj [c], Rita Traversi [d], Ilya Usoskin [e], Chen-Tung Arthur Chen [f], Jiann-Yuh Lou [g], Shuh-Ji Kao [c], Robert M. Carter [h], Valery Pipin [i], Mirko Severi [d], Silvia Becagli [d]

[a] Harvard-Smithsonian Center for Astrophysics, Cambridge, MA, USA
[b] Instituto de Geofísica, Universidad Nacional Autónoma de México, Ciudad Universitaria, 04510 México D.F., Mexico
[c] State Key Laboratory of Marine Environmental Science, Xiamen University, Xiamen, China
[d] Department of Chemistry "Ugo Schiff", University of Florence, Sesto F.no, 50019 Florence, Italy
[e] Sodankylä Geophysical Observatory and Department of Physics, University of Oulu, 90014, Finland
[f] Institute of Marine Geology and Chemistry, National Sun Yat-sen University, Kaohsiung, Taiwan
[g] Department of Marine Sciences, Naval Academy, Kaohsiung, Taiwan
[h] Institute of Public Affairs, Melbourne, Australia
[i] Institute of Solar-Terrestrial Physics, Russian Academy of Sciences, 664033 Irkutsk, Russia

ARTICLE INFO

ABSTRACT

We report on the existence and nature of Holocene solar and climatic variations on centennial to millennial time-scales. We introduce a new solar activity proxy, based on nitrate (NO_3^-) concentration from the Talos Dome ice core, East Antarctica. We also use a new algorithm for computing multiple-cross wavelet spectra in time–frequency space that is generalized for multiple time series (beyond two). Our results provide a new interpretive framework for relating Holocene solar activity variations on centennial to millennial timescales to co-varying climate proxies drawn from a widespread area around the globe. Climatic proxies used represent variation in the North Atlantic Ocean, Western Pacific Warm Pool, Southern Ocean and the East Asian monsoon regions. Our wavelet analysis identifies fundamental solar modes at 2300-yr (Hallstattzeit), 1000-yr (Eddy), and 500-yr (unnamed) periodicities, leaves open the possibility that the 1500–1800-yr cycle may either be fundamental or derived, and identifies intermediary derived cycles at 700-yr and 300-yr that may mark rectified responses of the Atlantic thermohaline circulation to external solar modulation and pacing. Dating uncertainties suggest that the 1500-yr and 1800-yr cycles described in the literature may represent either the same or two separate cycles, but in either case, and irrespective too of whether it is a fundamental or derived mode in the sense of Dima and Lohmann (2009), the 1500–1800-yr periodicity is widely represented in a large number of paleoclimate proxy records. It is obviously premature to reject possible links between changing solar activity at these multiple scales and the variations that are commonly observed in paleoclimatic records.

© 2014 Elsevier B.V. All rights reserved.

Contents

* Corresponding author.
E-mail address: wsoon@cfa.harvard.edu (W. Soon).

1. Introduction

In 1973, Denton and Karlen published a pioneering study of glacier expansion and contraction activity and associated tree-line fluctuations during the Holocene. Since then, numerous other paleoclimatic proxy studies have documented a rich pattern of Holocene climate variation and oscillation on multiple timescales. Our use of the terminology "centennial to millennial"[1] in description of such variability follows the order-of-magnitude tradition in geological literature, whereby the terms encompass several hundreds to several thousands of years.

Climatic rhythmicities[2] previously identified in proxy studies include the solar 50–100 year Gleissberg–Yoshimura cycle, a distinct 120-year cycle, the 200 year solar deVries–Suess cycle, the millennial Eddy cycle (see Kanda, 1933 for an earlier speculation of this scale identified based on ancient records of sunspots and auroras) and the bi-millennial Hallstattzeit rhythm. We recognize the Hallstattzeit signature in this paper at a periodicity of 2200–2400 years, which is consistent with its former identification at timescales of "~2000 year" by Obrochta et al. (2012), and of "~2400 year" by Vasiliev and Dergachev (2002) and "2500 year" by Debret et al. (2009) and Dima and Lohmann (2009). We also study other apparently derived climate modes on multi-centennial and millennial timescales include the well known 1500-year cycle as those proposed recently in Dima and Lohmann (2009).

Mayewski et al. (2004), Wanner et al. (2008) and Debret et al. (2009) have shown that the amplitudes of these centennial to millennial climate variations are quite large, generally accounting for between 10 and 30% of the total variance of a given paleo-time series. Mayewski et al. (1997) report that 40% of the variance of both the residual ^{14}C and the polar circulation index derived from the Greenland Ice Sheet Project 2 (GISP2) Holocene glacio-chemical time series can be explained by just the three bandpass-combined components of 2300 + 1450 + 512 year variability (see Fig. 9 of their paper).

Throughout this paper, we refer to 1500-yr or 1800-yr rhythms interchangeably because the underlying solar and climatic proxy records so far described do not have sufficient resolution to discriminate accurately between them. But we do consider the 1500-yr or 1800-yr solar-climatic rhythm to be statistically different from those of 1000-yr and Hallstattzeit period of 2200–2300-yr and hence a distinction useful for physical interpretation.

An important reason for studying millennial scale variation (or more generally any other repeating rhythmic timescale) is the possible use of the signals for diagnosing and contrasting between the competing physical processes that may have caused them. This was highlighted in the recent study by Konecky et al. (2013). Those authors showed evidence for the persistence of a millennial-scale intensification of the rainfall in southwestern Indonesia, through their precipitation proxy, δD_{wax}, from Lake Lading, East Java, and suggested that periods of higher rainfall were connected to the strengthening of the tropical Pacific Walker circulation. In contrast, if the precipitation signals were to be controlled by the migrations of Intertropical Convergence Zone (ITCZ) on multidecadal timescales, the authors suggested that they should have seen a drying tendency rather than seeing the rainfall increase persisting into the 20th century.

In seeking to better understand centennial to millennial solar and climatic cyclicities, we have deliberately restricted our study to Holocene time-series. In this way, we avoid the complexity of the ocean-atmosphere interactions with large ice-sheets that are known to be represented by the abrupt, warming–cooling Dansgaard–Oeschger events and their associated Heinrich events of iceberg discharges during the Late Pleistocene and earlier glacial periods. It is probable that the broad-band 1600-year pacing of the large and abrupt 8–16 °C warming, and the roughly equivalent 45 m of sea level rise that occurred during Dansgaard–Oeschger events (Schulz et al., 1999; Schulz, 2002; Pisias et al., 2010; Petersen et al., 2013), involve a different set of physical processes[3] than those that were operating during the Holocene. In addition, MacKay et al. (2013) have recently shown that millennial-scale variability during the Last Interglacial was more muted than Holocene variability, perhaps because of a diminished influence of freshwater discharge on the Atlantic Meridional Overturning Circulation (AMOC) during times of higher global temperature.

Our study of climate variability on intermediate, sub-orbital time-scales utilized the following techniques:

(1) The introduction of a new solar activity proxy based on nitrate concentration, using ice core data from Talos Dome, East Antarctica (Traversi et al., 2012). The physical reasoning is that nitrate concentration in polar regions, beside having tropospheric sources mainly located in low latitude areas, has a direct connection to the stratospheric production sources that result from the effects of solar irradiation and/or persistent modulation by extra-terrestrial fluxes of energetic particles (see for instance, Savarino et al., 2007).

(2) The development of a new multiple-cross-wavelet transform algorithm that is capable of incorporating multiple time series, a method that is akin to standard statistical multi-regression analysis.

(3) The deployment of this algorithm to study a range of hydro-climatic proxies from the North Atlantic Ocean, Western Pacific

---

[1] This term refers to orders of magnitude, i.e. to century-scale or millennial-scale, following an established usage in parts of the literature.

[2] We note that we have adopted and used phrases like "periodicities", "cyclicities", "oscillations", "timescales" and "rhythmicities" throughout the paper in the loose limit and constraint of our wavelet time–frequency analysis. Such use of course contrasts with the strict periodicity as often used and interpreted in the traditional Fourier transform sense. But we find that our usages stick more closely to the current state of our understanding of climate variations over the Holocene, rather than pretending any precise knowledge or definition of climate and its variations. We refer those readers interested in the rather poor state of development of climate theory in this regard to Essex (2011) and Essex (2013).

[3] One analysis and interpretation by Ditlevsen et al. (2005, 2007) concluded that Dansgaard–Oeschger events during glacial intervals are probably climate shifts that "are purely noise driven with no underlying periodicity". We assume no position nor view on this possibility because our study of millennial-scale variations during the Holocene strives to understand physical processes and mechanisms involved without the use of any particular favorite statistical models.

Warm Pool, Southern Ocean and East Asian Monsoon regions of the world ocean (see Section 2 for detailed descriptions).

We have deliberately chosen to analyze published Holocene time series whose wavelet spectral contents have not been previously studied, including: (i) a new Relative Gray Index (RGI) time series from Retreat Lake in Taiwan (previously unpublished); (ii) a Total organic carbon (TOC) content time series from sediments in the southern Okinawa Trough (Kao et al., 2005); (iii) a western Pacific warm pool sea surface temperature (SST) record (Stott et al., 2004); and (iv) a $\delta^{18}O$ record of two species of planktonic foraminifera (*Globigerina bulloides* and *Globigerinoides ruber*) from a sediment core collected from the Murray Canyon, off southern Australia (Moros et al., 2009).

(4) The identification of possible physical relationships that might link solar variability and climate variation on intermediate (i.e., multidecadal, centennial, multi-centennial and millennial) climatic timescales. In particular, intrinsic changes in the Sun's magnetic and radiative outputs may correlate with centennial to millennial patterns of change in climate proxy measurements, in a way that is quite distinct from the orbital changes in Sun–Earth precession, obliquity and eccentricity that provide climate forcing on scales of tens to hundreds of thousands of years. We made this assumption in our initial approach, but we note that our result may ultimately be expanded within the generalized stochastic-statistical frameworks of the so-called Hurst–Kolmogorov dynamics recently demonstrated and outlined by Markonis and Koutsoyiannis (2013).

In drawing our overall conclusions, we emphasize the multi-wavelength and broadband nature of the varied climatic responses to solar forcing (Wunsch, 2000; Markonis and Koutsoyiannis, 2013), and that intrinsically cyclic but aperiodic variations also exist in both the magnetic and radiative outputs of the Sun (see Gough, 1990; Tobias and Weiss, 2000; Gough, 2002; Usoskin et al., 2007; Spiegel, 2009; Weiss, 2011; Usoskin, 2013).

2. Methods and choice of data series

Table 1 lists a summary of the three solar activity and seven climate proxies that we study in this paper. Fig. 1 shows the time series of all these 10 time series in their original units and can serve as further clarification of the highly clumped, solar and climatic time series plotted at the top panels of Figs. 3 and 4, respectively.

2.1. Three Solar Activity Proxies: Nitrate Talos Dome Ice Core (TALDICE), solar modulation parameter from ^{10}Be and ^{14}C

We consider first the nitrate concentration record from TALDICE ice core (Talos Dome, East Antarctica, 72° 49′ S, 159° 11′ E, 2315 m a.s.l.), which covers roughly the last two glacial–interglacial cycles. The Talos Dome site is found to be suitable for retrieving a reliable data series for nitrate, at least in the Holocene period because its glaciological characteristics allow the preservation of this species in the snow layers (Stenni et al., 2002; Traversi et al., 2012). The nitrate content in such a favorable location is proposed to be mostly affected by changes of its production in the polar atmosphere by cosmic rays, and thus by solar activity, on multi-decadal to millennial time scales (Traversi et al., 2012). The link between nitrate in polar ice and solar activity is however still a debated issue, because multiple sources and post-depositional processes that affect nitrate make it rare to have available a fully reliable and long enough record to investigate its variability across all time scales from decadal to multi-millennial. Moreover, a complete model describing nitrate production and transport from the polar stratosphere is not available so far. Here, however, we stress that the relation between nitrate and solar activity on the long-term scale is completely different from that caused by solar energetic particle events on the time

Table 1

List of various solar and climatic proxy records (see Fig. 1 for all the ten time series) subjected to wavelet analysis in the present study.

| Name of dataset	Location (with altitude/water depth)	Start date (BP)	End date (BP)	Resolution (years)	Proxy used	Reference
TALDICE Antarctic ice core	Talos Dome, East Antarctica 74°49 S, 159°11 E 2315 m a.s.l.	645	11,400	12–30	Nitrate (NO^-_3)	Traversi et al. (2012)
Retreat Lake Core R, Taiwan	Retreat Lake, NE Taiwan 24°29′30″N, 121°26′15″ E 2230 m a.s.l.	5	9812	1–10	Relative Gray Index (RGI)	Selvaraj et al. (2007, 2011)
IMAGES VII Core MD012403	Southern Okinawa Trough 25.07° N, 123.28° E, 1420 m	157	32,513	84–913	Total organic carbon (TOC)	Kao et al. (2005)
Solar Modulation Function	Greenland Ice Core Project (Summit, Central Greenland)	329	9279	25	^{10}Be	Vonmoos et al. (2006)
^{14}C	Worldwide (IncCal98)	85	11,405	10	^{14}C	Usoskin and Kromer (2005); Usoskin et al. (2007)
Iceland-Scotland Overflow Water	Gardar Drift, South Iceland Basin	0	10,388	25–211	Sortable silt mean size (10–63 μm)	Bianchi and McCave (1999)
(ISOW) Record Cores NEAP-15 K and NEAP-16B	56°21.92′ N, 27°48.68′ W, 2848 m					
Holocene stacked Records of drift ice	Northern North Atlantic Region	0	10,550	70	Percentages of lithic grains or Ice-rafted debris	Bond et al. (2001)
Core MC52	55°28′ N, 14°43′ W, 2172 m					
Core VM29-191	54°16′ N, 16°47′ W, 2370 m					
Core MC21	44°18′ N, 46°25′ W, 3959 m					
Core GGC22	44°18′ N, 46°25′ W, 3958 m					
West Pacific Warm Pool SST Stack	Western Tropical Pacific Ocean off Indonesia	125	14,875	250	Mg/Ca derived SST record	Stott et al. (2004)
Core MD81	6.3° N, 125.83° E, 2114 m					
Core MD76	5°00.18′ S, 133°26.69′ E, 2382 m					
Core MD70	10°25.52′ S, 125°23.29′ E, 832 m					
Murray Canyon, South Australia Core MD03-2611	Murray Canyon off South Australia 36°43.8′S, 136°32.9′E, 2420 m	0	10,984	38	G. bulloides $\delta^{18}O$	Moros et al. (2009)
Murray Canyon South Australia Core MD03-2611	Murray Canyon off South Australia 36°43.8′S, 136°32.9′E, 2420 m	0	10,984	38	G. ruber $\delta^{18}O$	Moros et al. (2009)
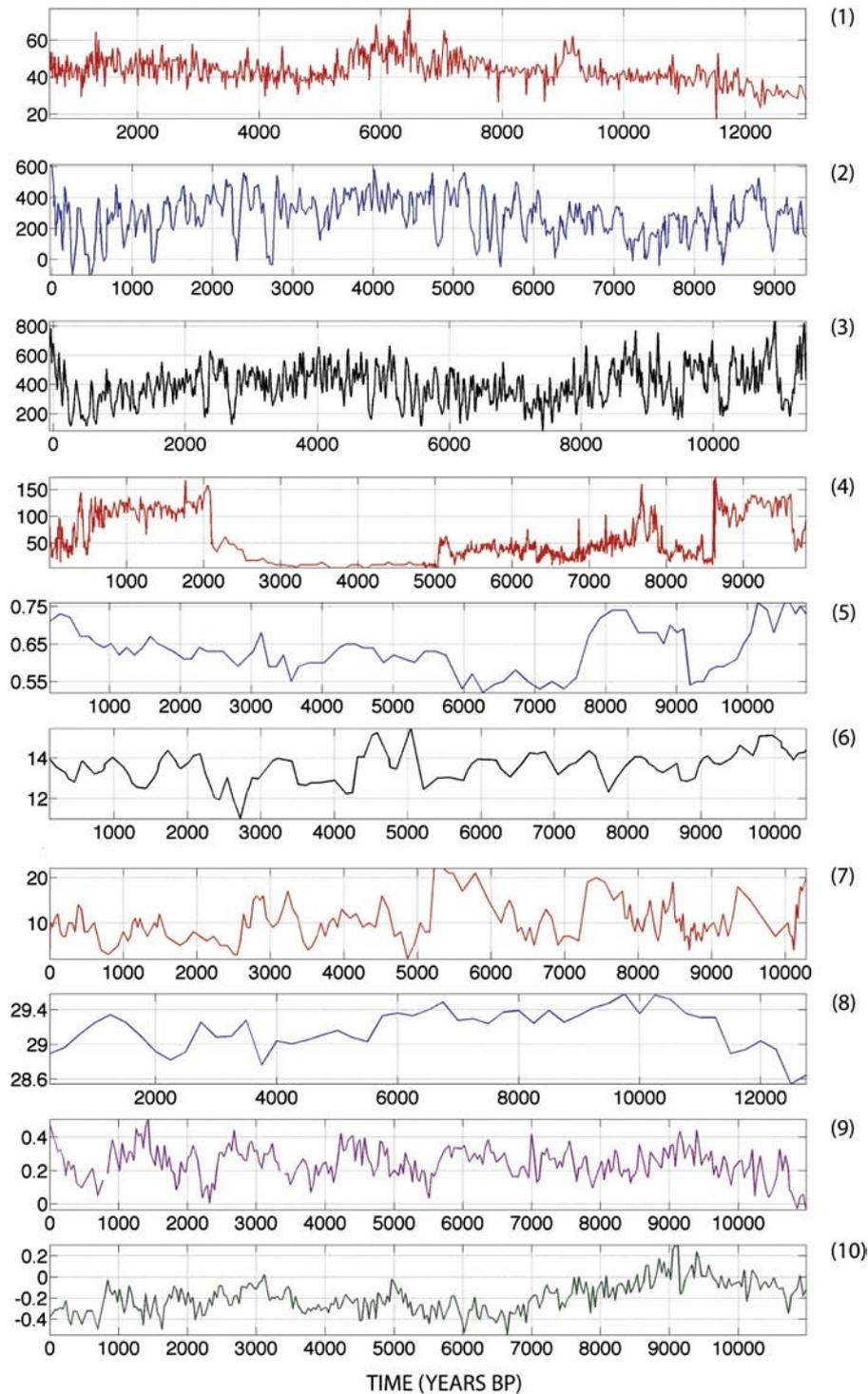
Fig. 1. The time series for the 3 solar activity proxies [(1) Nitrate, (2) ^{10}Be, and (3) ^{14}C] and 7 climatic proxies [(4) Relative Gray Index-RGI, (5) Total Organic Carbon-TOC, (6) Sortable Silt mean size, (7) Hematite stained grains-HSG, (8) Sea surface temperature-SST, (9) *G. bulloides* δ^{18}O, and (10) *G. ruber* δ^{18}O] over the Holocene used in this study. The original sources for these time series are summarized in Table 1.

scale of days-weeks-months (McCracken et al., 2001). The very short-term connection between solar activity and ice core nitrate has been disputed by the recent work of Wolff et al. (2012), where nitrate records from Antarctic and Greenland ice cores covering the time of the Carrington event (September 1–3, 1859) were taken into account. No large nitrate spike was found in the considered Antarctic cores around 1859 whereas the large nitrate spikes observed at that time in Greenland cores were ascribed to bio-mass burning events occurred in Europe. The paper by Wolff et al. (2012) seriously challenges the possibility of using nitrate in polar ice as specific proxy of solar energetic events, although only a selection of the many available highly resolved records from Antarctica and Greenland was considered and the potentiality of nitrate record from the Antarctic Windless Bight ice core (McCracken et al., 2001) was not ruled out. Hence, this possible solar energetic particle event and nitrate connection has been put into question but not definitively resolved yet.

Traversi et al. (2012) have recently stressed that nitrate concentration has the potential to be used as a plausible and reliable tracer of

solar magnetic variations on a wide range of timescales (see also Laluraj et al., 2011). Ogurtsov and Oinonen (2014) recently reported "distinct century-scale (50–150 yr) variability" in nitrate record of Laluraj et al. (2011) from East Antarctica and another record from Central Greenland. Based on this assumption of solar activity-nitrate link, Traversi et al. (2012) have shown that nitrate concentration yields higher correlations and coherency with the two cosmogenic isotopes that represent standard solar proxies (^{14}C and [10]Be) than with any regional climate proxies (see the results in Table 1 of that paper). We shall also adopt this general assumption, and we provide below additional analysis and discussion on the connection of nitrate to both the solar modulation parameter, Φ (see the formalism in Usoskin et al., 2005), derived from [10]Be of the Greenland Ice Core Project (Vonmoos et al., 2006), and to ^{14}C production rates (Usoskin and Kromer, 2005; Usoskin et al., 2007), especially at the 1000, 1500–1800 and 2300 year timescales.

Using firn core data, Traversi et al. (2012) have already related solar activity signals in the nitrate proxy to the modulation of the 11-yr Schwabe and 50–100-yr Gleissberg–Yoshimura cycles, but strong inter-annual meteorological noise makes the detection and resolution of such cycles hard to confirm.[4] This is why we have focused our study on ice core samples from 73 to 665 meter depth, roughly corresponding to the Holocene interval from 560 to 11,400 years BP. The sampling resolution across this interval averages 20 years.

We have also assumed in this study that all three of the solar activity proxies adopted represent intrinsic changes in the Sun's magnetism. At the same time, we leave open the question posed by St-Onge et al. (2003) as to whether plausible coherence exists between the Earth's relative paleomagnetic intensity index and the [10]Be and ^{14}C-related time series on 1250-yr and 420-yr timescales. The recent picture sketched by Panovska et al. (2013), who suggested that Holocene geomagnetic records possessed not discrete periods but a continuous broadband spectrum with a power law exponent of −2.3 ± 0.6 for periods from 300 to 4000 years, certainly add a healthy dose of caution to any simplistic interpretation or premature conclusion.

2.2. Choice of Holocene paleoclimatic time series from regions of the East Asian Monsoon, North Atlantic Ocean, Western Pacific Warm Pool and Southern Ocean

2.2.1. Relative Gray Index (RGI) time series (Retreat Lake, Taiwan)

The RGI is a measure of the degree of sediment lightening or darkening, and usually reflects the relative proportion of organic to inorganic/minerogenic materials present in sediments. In the subalpine lake sediments of Taiwan, this ratio primarily depends on the catchment vegetation type (C_3 and C_4), as well as the intensity of erosion and weathering of rocks in the catchment; both processes are intimately related to the strength of the East Asian monsoon (EAM). For these reasons, we interpret the RGI data as a proxy for the varying intensity of the summer component of EAM conditions in subtropical Taiwan (Lou and Chen, 1997).

On our adopted RGI scale of 0 (dark) to 255 (white), higher RGI values (>80–170) between ~170 and 155 cm and in the top ~45 cm of the time series studied, indicate the presence of lighter (TOC content ~ 2% with lower C_3/C_4 ratio) more minerogenic (Al content ~8–10%) sediment during the early and late Holocene intervals, respectively. These intervals correspond to cool-wet and cool-dry climates and a relatively weak EAM in subtropical Taiwan. By contrast, the low RGI values (<80) that characterize sediments between ~155 and 45 cm of the core identify the presence of organic-rich (TOC content ~40% with higher C_3/C_4 ratio), peaty sediments. The dark, peaty sediments cored in Taiwan indicate the presence of dense C_3 vegetation in the catchment, which is nourished during strong monsoon seasons. In turn, the same monsoonal signal is reflected by enhanced total organic carbon content and a lowered carbon isotope ($\delta^{13}C$) value, as shown by earlier

measurements on sediments from the same lake (Selvaraj et al., 2007, 2011). Our interpretation of such paleoclimatic proxies is broadly similar to vegetation changes during the Holocene that have been described from South Korea (see e.g., Lim et al., 2012, 2013).

The RGI record from Retreat Lake provides a complete Holocene record at better than decadal resolution. The record documents the presence of a mid-Holocene period of optimum climate (~7500–5500 cal yr BP), when enhanced monsoonal activity occurred, and a number of weak monsoon intervals before ca. 9400 and at 8200, 6900, 5500–4500 and 3500 cal yr BP, some of which also occur in other high resolution Asian monsoon records (e.g. Gupta et al., 2003; Wang et al., 2005).

2.2.2. Total Organic Carbon (TOC) time series (Okinawa Trough)

A Holocene TOC time series has been reconstructed from a piston core (MD012403) raised by RV *Marion Dufresne* during May, 2001 from a water depth of 1420 m in the southern part of the Okinawa Trough (122.28° E, 25°07 N) (Kao et al., 2005). The core chronology back to the Last Glacial Maximum (LGM) has been firmly established based upon accelerator mass spectrometry radiocarbon (AMS ^{14}C) dating of planktonic foraminifers (*Globigerinoides* and *Orbulina universa*).

Based on the sedimentary TOC, TOC/total nitrogen (TN) ratio and total sulfur (TS) time series, Kao et al. (2005) observed low TS content in sediments of the Holocene compared to sediments of the last glacial period. Further they showed that low TS content during the Holocene was not controlled by TOC (refer Fig. 2 in Kao et al., 2005), since the TOC content of marine sediments primarily represents residual organic material that has been oxidized to varying degrees along a variety of pathways (i.e. oxygen, iron and sulfate). Although the Okinawa TOC content varied insignificantly after the LGM, distinctly low TS content in the Holocene part of the core indicates that less organic material was mineralized via sulfate reduction then, which in turn can be inferred to result from an intensification of the Kuroshio Current (KC), together with a parallel enhancement of deepwater circulation.

By providing additional oxygen to maintain a higher redox potential at the sediment water interface, such oceanographic conditions diminished sulfate reduction during the Holocene, a time when the East Asian monsoon was also intensified as a result of increased Northern Hemisphere insolation (Berger and Loutre, 1991). Therefore, the increased EAM inferred from the RGI record from Taiwan and the intensified KC phases implicated from TOC and TS records from the southern Okinawa Trough act in the same direction as the KC. Together, these processes carry huge amounts of heat from the equatorial Pacific to the northern North Pacific; thereby, strongly influencing climate over a wide region of East Asia and the northwest Pacific Ocean.

Noting these climatic links, we selected the RGI and TOC time series for wavelet analysis in order to identify any periodicities that may pertain to climate-forcing mechanisms, and especially to solar forcing of the East Asian monsoonal hydroclimate during the Holocene.

2.2.3. Other time series

In addition to the RGI record from Retreat Lake and TOC record from Okinawa Trough, we have also included in our analysis several other key climatic and oceanic proxies. These are derived from the North Atlantic Ocean – the sortable silt index (SSI) time series of Bianchi and McCave (1999) and the 4-records stacked drift ice index of Bond et al. (2001), the western Pacific Warm Pool – the 3-core records stacked sea surface temperature (SST) series of Stott et al. (2004), and the Southern Ocean – time series of $\delta^{18}O$ in *Globigerina bulloides* and *Globigerinoides ruber* from a deep sea sediment core collected from Murray Canyon off South Australia by Moros et al. (2009).

2.2.4. Multiple-Cross-wavelet for time-frequency analysis with multiple time series

We introduce here a new algorithm that is designed to analyze multiple time series in time-frequency space. This algorithm is clearly a more efficient and effective method of examining common and

---

[4] It is also clear that the detection of any periodicities depend on the quality of datasets and the methods of analysis adopted.

coherent signals in multiple time series than was able to be provided by previous, simpler algorithms that only allow computation based on information from amplitude of each time series. Some brief introduction and discussion of using wavelet transform for time series analysis can be found in Frick et al. (1997) and Soon et al. (1999).

Here we use the Morlet wavelet as the mother function ($\psi_0(\eta)$) because it provides a higher periodicity (frequency) resolution and because it is complex, which allows us to calculate the phase information (Soon et al., 2011). The Morlet wavelet $\psi_0(\eta)$, which consists of a complex exponential function modulated by a Gaussian, is defined as:

$$\psi_0(\eta) = \pi^{\frac{-1}{4}} e^{i\omega_0 \eta} e^{\frac{-\eta^2}{2}}$$

where η is a nondimensional "time" (Torrence and Compo, 1998). For the Morlet wavelet to be a mother wavelet, it must have finite energy and a zero mean (i.e., satisfying the admissibility condition, $\omega_0 = 6$ (Farge, 1992).

The cross wavelet analysis, as introduced by Hudgins et al. (1993) and defined for two time series X_1 and X_2, with wavelet transforms (W_{X_1}) and (W_{X_2}), respectively, is:

$$W^{X_1 X_2} = W_{X_1} W_{X_2}^*,$$

where (*) denotes complex conjugation. Torrence and Webster (1999) defined the cross-wavelet energy as, $\left| W_n^{X_1 X_2} \right|^2$.

For analysis of two (X_1 and X_2) or more time series ($X_1, X_2, X_3,..., X_m$), the multi cross-wavelet was used which measures the common power among these time series accounting for the synchronization in phase, frequency and/or amplitude.

We define the multiple cross wavelets as:

$$W^{X_1, X_2, X_3, ..., X_m} = \left\langle W_{F_i} \prod_{k=1}^{n} W_{G_k}^* \right\rangle,$$

where $F(t)$ and $G(t)$ are matrices within which each element represents a time-dependent function itself and $< \cdot >$ indicates an average of the multiple cross wavelets.

The phase angle of $W^{X_1, X_2, X_3, ..., X_m}$ describes the phase relationship between the $X_1, X_2, X_3,...,$ and X_m series in time–frequency space. The statistical significance of the multiple-cross wavelet is estimated using Monte Carlo methods with red noise to determine the 5% significance level (Torrence and Webster, 1999).

The arrows in the multiple-cross-wavelet spectra show on average the degree of linear or nonlinear dependence between the $X_1, X_2, X_3,...,$ and X_m in time–frequency space and the phase among these time series: arrows at 0° (pointing to the right) indicate that both time series are perfectly positively correlated (in phase) and arrows at 180° (pointing to the left) indicate that they are perfectly negatively correlated (180° out of phase). It is important to understand that these two perfect cases imply a linear relationship between the considered phenomena. Non-horizontal arrows indicate an out of phase situation, meaning that the studied phenomena have a more complex non-linear relationship.

The mathematical basis of the new multiple-cross-wavelet algorithm is a generalization of Wiener (1930)'s original cross function, but we compute in time–frequency space. Also, instead of considering the functions F and G, we consider two matrices $F(t)$ and $G(t)$. We describe in the Appendix A the details of our new algorithm, together with calculations and some tests that have been applied to it.

3. Results and discussion

3.1. Wavelet spectra of three solar proxies

Fig. 2 shows the wavelet spectrum for the new solar activity proxy based on nitrate concentration. Concentrations of power occur at 3358-yr and 1585-yr, across a broad-band peak that ranges from about 900-yr to 500-yr, 120–140-yr, and at roughly the Gleissberg–Yoshimura 50–100 yr periodicity. All of these frequencies are potentially physically relevant for linking climate to intrinsic variations of the Sun's magnetic activity. We note that both the 1585-yr and 50–100-yr cycles present in the solar nitrate proxy agree with previously recognized solar periodicities, namely the 1500-yr and 93-yr periods found for a surface salinity proxy from Florida Straits for the early-to-mid Holocene interval of 9.1 to 6.2 kyr BP (Schmidt et al., 2012; these authors also identified 87-yr and 60-yr peaks in their high-resolution data series). Using the solar modulation potential function for the past 9400 years, determined from the two cosmogenic radionuclides ^{10}Be and ^{14}C, Abreu et al. (2012) found the periodicities of 88, 104, 150 and 506 years using the Fourier Transform method and Hanslmeier et al. (2013) using wavelet analysis reported the period of about 1000 years, Velasco Herrera (2013) also applying wavelet transform found periodicities of 60, 128, 240, 480, 1000 and 2100 years.

The most surprising and novel aspect of our results in Fig. 2 is the detection of 1500-yr cycles in a new solar activity proxy record. We make this identification cautiously because it is not yet fully established that this periodicity is physically connected to solar magnetism, despite the encouraging presence of 1500-yr cycles in a recent toy-model of a nonlinear solar dynamo (Pipin et al., 2012). Brandenburg and Spiegel (2008), using another toy αω-dynamo model, have provided evidence for the possible existence of 200–500 year solar magnetic variation, a frequency that is observed when their model is parameterized to adjust for the long-term memory of the so-called α-effect. It remains a challenge for solar physics to fully explore, and demonstrate the robustness of, the possible 200–500 year and likely 1500-yr quasi-regular oscillations in the Sun's magnetic and radiative outputs. In the meantime, however, little doubt now exists that fluctuations at these intervals are present in proxy-climate datasets.

In general, the solar dynamo theory supports the idea that long-term quasi-periodic variations of solar magnetic activity can result from the nonlinear interplay between the magnetic field, differential rotation and helical convective motions. The most important timescales are related to the time taken to re-establish the angular momentum balance (differential rotation) and the magnetic helicity balance (associating with the α-effect) in the convection zone caused by perturbations in the large-scale magnetic field. Both processes, i.e. relaxation of the angular momentum transport and the magnetic helicity balance, correspond to about 10 solar cycles (see, Pipin, 1999; Pipin et al., 2012). Pipin et al. (2012) also found that a combination of the random fluctuations of the dynamo governing parameters and the nonlinear relaxation of the principal dynamo mechanisms can produce the quasi-periodic variations on millennial timescales. However, the stability of the revealed periods can be questioned, because the dynamo may become non-stationary under random fluctuations. Moreover, it happens that the dynamical properties of the solar dynamo on the millennial timescale look very similar to the properties of the Brownian motions (Pipin et al., 2013). This is another reason why we think our current choice of subjective wordings in describing solar and climate variations as noted under footnote 3 is more physically accurate and honest than any deliberate attempt to impose a falsely precise vocabulary.

Given the relatively short time series considered in Fig. 2 (or see Fig. 1 for all the ten series), the prominent 3358-yr peak in the nitrate solar activity proxy (Fig. 2) may be given less scientific weight. However, results from previous researchers suggest that it may also represent a real feature. For example, Stuiver et al. (1995) have recorded a 3300-yr period in their Holocene bidecadal-resolution record of δ^{18}O from GISP2, and Mayewski et al. (1997) reported a highly significant peak at 3200-yr in a record of Holocene polar circulation. Cleroux et al. (2012) show the presence of the 3300-year period for a δ^{18}O$_{seawater}$ Holocene series from the sediment core off Cape Hatteras (although the 3300-yr scale obviously lies outside the cone-of-influence of their wavelet analysis where edge effects, owing to a finite length of time series, become important). Finally, a roughly 3000-yr
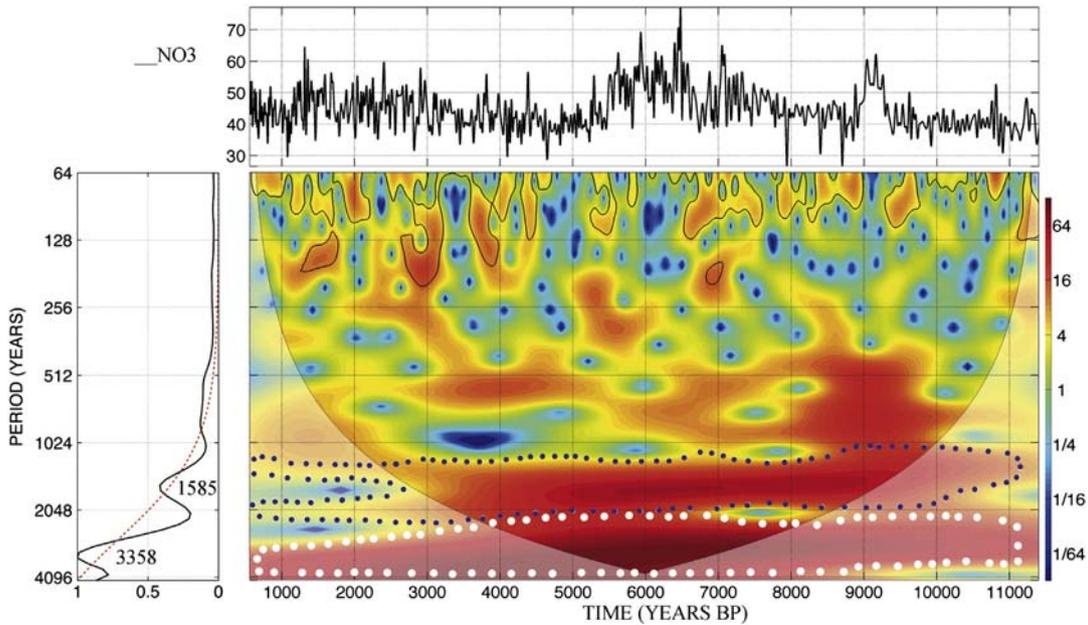
Fig. 2. Wavelet transform analysis of the newly proposed solar activity proxy, nitrate concentration from TALDICE ice core (Traversi et al., 2012), time series from 11,400 to 560 years BP (shown as black curve in the top panel) illustrating the wavelet powers at centennial to millennial timescales (center panel). Dotted blue/white contours highlight some of the millennial periods, including especially the 1500- to 1800-yr scale, discussed in this paper. The left panel shows the global spectrum of the wavelet power averaged over time. Dashed line represents the significance level referenced to the power of red noise level at the 95% confidence interval. Shaded regions outline the cone of influence limit where the calculated wavelet powers can be distorted (hence less reliable) owing to the "edge"-effects of any time series. (For interpretation of the references to color in this figure legend, the reader is referred to the web version of this article.)

period has also been detected in a lacustrine sedimentary proxy for storminess in the Northeastern United States (Noren et al., 2002).

Fig. 3 shows the results of our analysis of the three most significant solar activity proxies that are available for the Holocene: namely nitrate concentration at Talos Dome, the Solar Modulation Parameter, Φ, based upon [10]Be analyses from the Greenland Ice Core Project, and the Solar Modulation Parameter, Φ, based upon ^{14}C production rate from the accurate annually-dated tree-ring chronology. In studying the wavelet-transform results in Figs. 3 and 4, it is important to consider not only the peaks in the time-averaged global spectra (left panel in each figures)
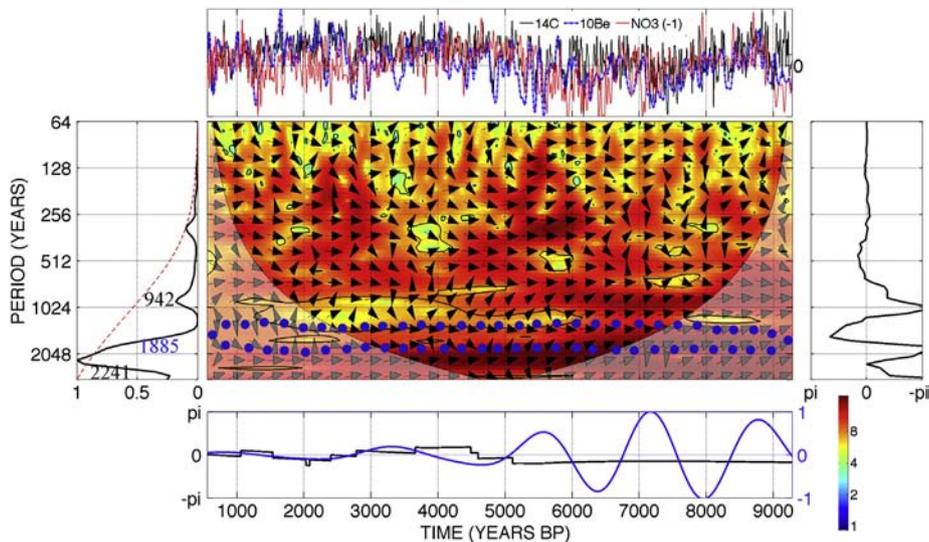

Fig. 3. Results of the multi-variable cross wavelet analysis of the three solar activity proxy time series: Nitrate concentration (Traversi et al., 2012; red series in top panel), Solar Modulation Parameter, Φ, derived from [10]Be of the Greenland Ice Core Project (Vonmoos et al., 2006; blue series in top panel) and from ^{14}C production rate (Usoskin and Kromer, 2005; Usoskin et al., 2007; black series in top panel). Dotted blue contours highlight the 1885-yr millennial period discussed in details in the main text. The orientation of the arrows shows relative phasing of the time series at each timescale; arrows at 0° (pointing to the right) indicate that both time series are perfectly positively correlated (in phase) and arrows at 180° (pointing to the left) indicate that they are perfectly negatively correlated (180° out of phase), both of these two perfect cases implying a linear relationship between the considered phenomena; non-horizontal arrows indicate an out of phase situation and a more complex non-linear relationship (see Appendix A for further explanation). This result seeks to establish the baseline, oscillatory timescales common to all three solar activity proxies in order to allow a better interpretation of physical bases and processes involved in several climate variation signals, including those representing the East Asian monsoon and the Arctic–North Atlantic meridional overturning circulation systems (see further results and discussion in Fig. 3). Additional features in this figure are explained in the caption for Fig. 2 and in the Appendix A. Unlike in Fig. 2, we added the information of the global phase (right panel) averaged over time and the instantaneous phase (black curve) and amplitude (blue curve) for the 1400–2000-yr bandpassed scale over the Holocene (bottom panel). The result shows a rather in-phase and linear relationship among the 3 solar activity proxies but a highly time-dependent nature of the amplitude of the millennial scale variation. (For interpretation of the references to color in this figure legend, the reader is referred to the web version of this article.)
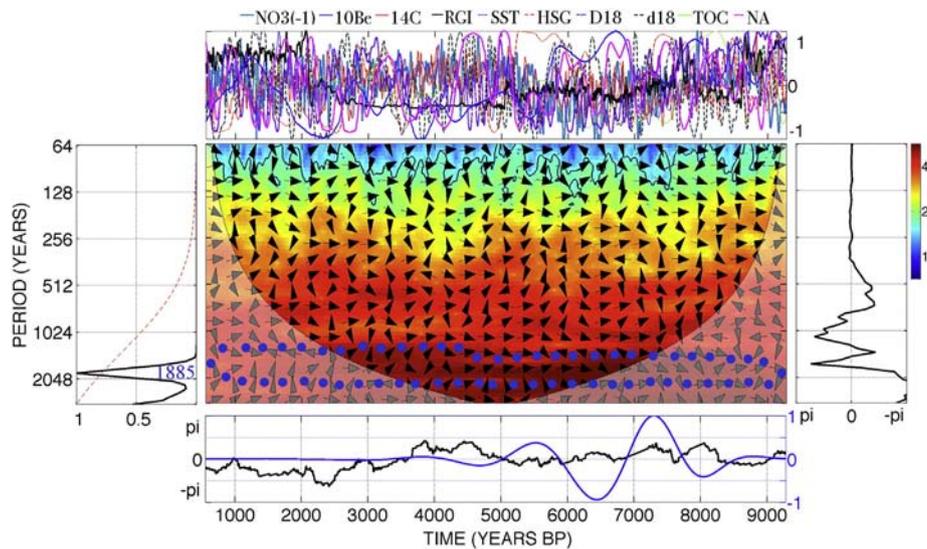
Fig. 4. Results of the multi-variable cross wavelet analysis of the nitrate, [10]Be and ^{14}C solar activity proxies and a total of seven paleoclimatic series from the North Atlantic (sortable silt mean size series from Bianchi and McCave, 1999; and stacked drift ice indices in Bond et al., 2001), Western Pacific Warm Pool (stacked SST series from Stott et al., 2004), East Asian Monsoon (Relative Gray Index series from Retreat Lake in Taiwan and Total organic carbon content in sea sediment from Okinawa Trough; see Kao et al., 2005) and Southern Ocean (δ^{18}O in *Globigerina bulloides* and *Globigerinoides ruber*, from deep sea sediment core at Murray Canyon off southern Australia; see Moros et al., 2009). Dotted blue contours highlight the 1500–1800-yr time scales discussed in this paper. For explanation of arrow orientations, see caption to Fig. 3, and the Appendix A. Additional features in this figure are explained in the captions for Figs. 2 and 3. (For interpretation of the references to color in this figure legend, the reader is referred to the web version of this article.)

but also the instantaneous time-frequency spectra shown in the central panel of Figs. 3 and 4.

Several prominent common signals occur in Fig. 3. First, the signal of the 1885-yr periodicity has strong time dependence in the amplitude of its variation, with relatively larger amplitude during the early to mid-Holocene and relatively muted amplitude for late Holocene (see blue curve in the bottom panel of Fig. 3). This signal can only be obtained using the unique, inverse multiple cross wavelet transforms presented here. It is important to highlight the fact that a common 1800-yr solar variation timescale has been captured by three very different solar proxies which represent different geographic and climatic parts of the Earth's climate system. The most important result concerning the 1800-yr scale variation from Fig. 3 is its relatively in-phase or linear relationship (see black curve in the bottom panel of Fig. 3) for the three different solar activity proxies. This result, in turn, emphasizes the pacemaker role of the solar activity forcing on millennial scale rather than any strict persistence from the sense of amplitude modulation through the solar radiative forcing on Earth climatic responses.

Our independent result therefore reaffirms the conclusion and analyses in Traversi et al. (2012), and our conclusion on the clear time-dependence of the amplitude of the 1885-yr millennial scale variation is also broadly consistent with the previous results of Debret et al. (2007, 2009).

If only one of the solar proxies showed a coherence at ~1800-yr with climatic indices, this might reflect a regional climatic influence upon the proxy record. However, since all the three proxy series show a similar relation, and since each has quite a different fate in the terrestrial system (nitrate are expected to be mostly affected by the tropospheric air mass transport and snow deposition in Antarctica; [10]Be—by stratospheric air mass transport and snow deposition in Greenland; [14]C—mostly by the global ocean circulation), a tripartite simultaneous influence of regional climate on the proxy data sets is unlikely. Accordingly, we view the 1500–1800-yr scale as representing a fundamental periodicity of the spectrum of solar variation rather than a mere derived mode in the framework of Dima and Lohmann (2009; see further discussion in Section 3.2 and 3.3 below).

Fig. 3 also exhibits significant spectral power on timescales of 2200–2400-yr, 1000-yr, 500–700-yr, 350-yr, 120-yr and 50–100-yr. Almost without exception, the amplitudes of all these periodicities

vary over time during the Holocene. This empirical observation implies a very rich nonlinear interaction for the relevant underlying physical processes and dynamics, without the predominance of any particular operational timescales.

3.2. Wavelet spectra of individual paleoclimatic data-series

Before discussing the master multiple-cross-wavelet analysis based upon the three solar proxy time series and seven paleoclimatic records (Section 3.3 and Fig. 4), we comment first on the wavelet spectra that occur in some of the individual climate proxies used in this study, since most of them have not been previously published and discussed.

First, wavelet analysis of δ^{18}O in the *Globigerina bulloides* record identifies a dominant 1585-yr scale power, which is closely similar to the 1567-yr signal reported previously using conventional Fourier-based time series analysis (Moros et al., 2009). The wavelet analysis also identifies a further significant concentration of power at about 560-yr in this series. Applying wavelet analysis to the available δ^{18}O record for the planktonic species *Globigerinoides ruber* from the same sediment core identifies prominent concentrations of power at about 2048-yr, 1000-yr and 512-yr, consistent with our other results and with solar activity forcing.

Second, direct wavelet analysis of the composite Western Pacific Warm Pool SST time series (binned MD81, MD 76 and MD 70 Holocene series) of Stott et al. (2004) also identifies a convincing signal at the 1800-yr scale that persists throughout the Holocene. A similar 1800-yr variability is also found in the East Asian monsoonal RGI index from Retreat Lake, and an 1800-yr periodicity also appears in the Holocene wavelet spectrum for the SST-Mg/Ca proxy from Cape Hatteras published in Cleroux et al. (2012). Finally, the direct wavelet analysis of the sortable silt size time series (a direct proxy for the North Atlantic THC/AMOC) from the NEAP-15 K core in Bianchi and McCave (1999) yields not only a prominent 1400-yr periodicity, but also significant peaks at 700-yr and 2700-yr scales.

Fig. 4 presents these results, and the co-variations of all the solar and climatic proxy series, in compact form in a single chart. With the aid of the new multiple-cross-wavelet algorithm, we have been able to study, in a consistent way and for the first time, the common signals contained in three different solar activity proxies (nitrate concentration and solar

modulation parameter, Φ, from [10]Be and ^{14}C discussed in Fig. 3) and in seven climate proxy time series which cover geographical regions and climatic regimes from the North Atlantic Ocean, East Asia, the Western Pacific Warm Pool area and the Southern Ocean. It should be noted, of course, that the illustrative results shown in Fig. 4 are an incomplete representation of 1500–1800 year co-variations for the whole globe (see the fuller list in the references cited in Section 3.3 below: we have deferred the most complete assembly and analysis of this 1500–1800 yr variation to future studies).

In Fig. 4, the 1885-yr scale periodicity is very prominent and persists throughout the entire Holocene, and another broadband concentration of power at 500–1200-yr timescales is also noteworthy. The relative phase information (indicated by the black curve shown in the bottom panel of Fig. 4), indicates that the common signal for the 1885-yr co-variations are somewhat linear for the combined total of ten solar and climatic time series. The results are nonetheless consistent with the rectification of solar activity forcing by the North Atlantic THC/AMOC threshold-dependent filter, as outlined by Dima and Lohmann (2009).

Our results, and especially those represented by Fig. 4, suggest periodic/rhythmic suborbital-scale variability of both solar activity and of climatic proxies is the general rule rather than exception during the Holocene. Rejection of a sun-climate connection, for example on the 1500-yr or 1800-yr timescales, by demanding that a stronger solar forcing is required is simply untenable given the known operation of nonlinear physical processes that can delay, rectify or modulate a solar-originated signal (see also e.g. Weng, 2012a,b). For example, and as already discussed by Dima and Lohmann (2009), rectification by the Atlantic THC/MOC deep-water circulation can produce a 1500-yr or 1800-yr signal in climate proxies even though the original solar forcing may not contain a 1500-yr or 1800-yr cycle, or at best an extremely low-amplitude one. In accepting the existence of a persistent solar forcing on the 1500-yr and 1800-yr scales, we are simply accepting a reality that has long been known to paleoceanographers like Bianchi and McCave who have emphasized the importance of "an oceanic internal oscillation in conveyor strength" (e.g. Bianchi and McCave, 1999). In this sense, the scenario of a "wobbly ocean conveyor circulation" as sketched by Denton and Broecker (2008) should also be studied carefully, especially in terms of the full list of paleoclimatic evidence for millennial-scale climate variations across the whole globe assembled under Section 3.3 below.

Finally, we should comment on the plausible, though rather improbable, claimed link between 1800-yr climatic variability and tidal forcing by the nearby Moon, as hypothesized by de Rop (1971) and Keeling and Whorf (2000). We prefer instead the careful conclusions reached by Munk et al. (2002, p. 370), who interpreted the 1800-yr periodicity as representing the repeated co-alignment of the Sun, Moon and Earth. Regarding this, Munk et al. assert that the "[t]idal forcing is very weak and an unlikely candidate for millennial variability; the Keeling and Whorf proposal is considered as the most likely among the unlikely candidates."

3.3. Solar-related variability on centennial and millennial scales

In their discussion of the 1500-yr or 1800-yr climatic cycle, which many writers assign to a solar origin, Dima and Lohmann (2009) introduced the distinction between fundamental and derived modes of climatic variation. They consider a fundamental mode to be one that is forced directly by changes in solar output which correspond to an associated physical mechanism. In contrast, a derived mode is one that has no necessary solar physical process operating at its characteristic timescale, but instead represents the rectification of a solar forcing by an intermediate dynamic planetary mechanism (such as oceanic oscillation). In such a fashion, a derived mode results from the linear representation in Fourier space of non-linearly transformed fundamental modes. The ~1500-yr "solar" cycle, and the associated Dansgaard–Oeschger and

Heinrich events,[5] were proposed by Dima and Lohmann to represent an internal threshold response of the global thermohaline circulation to solar forcing, and thus to represent derived climatic modes.

Our results herein fit well with the Dima and Lohmann analysis, and their insightful distinction has the capability to lead to a correct interpretation for solar phenomena that have been perceived on a wide variety of timescales, through the interaction of solar forcings and large planetary-scale systems such as the THC or AMOC. Although it is worth repeating that we have focused strictly on solar and climatic variations over the Holocene.

Regarding the 1500-yr or 1800-yr cycle in particular, our results are also generally consistent with other recent analyses (e.g. Debret et al., 2009; Darby et al., 2012; Obrochta et al., 2012; Sorrel et al., 2012). Nonetheless, and bearing Dima and Lohmann's distinctions in mind as well as our new results shown in Figs. 2 and 3, we suggest that it is premature to reject yet the possibility that the ~1500-yr or ~1800-yr climatic-THC variation may be connected to intrinsic variations in solar radiative and charged-particle output. Our reason for this is simply that the proximate 1500-yr or 1800-yr scale periodicity appears in the wavelet spectra of both the nitrate-based (Fig. 2) and combined 3-record-based (Fig. 3) solar activity proxies analyzed in this paper (and, earlier, at a "1600-yr" scale for both the ^{14}C production rate and [10]Be-related time series in Debret et al., 2007), despite the fact that the signals may not persist through the entire Holocene. These thoughts notwithstanding, we wish to highlight that the nonlinear climate dynamics framework of Dima and Lohmann (2009) also provides a clear alternative physical basis for a 1500-yr cycle to be associated with climatic responses across the globe without any necessity for an actual persistent solar forcing at that periodicity.

Irrespective of its fundamental or derived nature, a solar-related character for the 1500-yr or 1800-yr periodicity is consistent with the fact that almost all of the proposed millennial-scale solar-climate connections correspond to quasi-regular repetitions of weaker solar activity/low solar irradiance. The effects of this include periods of colder temperature, expansion of glacier ice-mass or sea-ice, increased ice-drafted debris, increased storminess and a more negative Arctic Oscillation index. Other specific responses that have been documented include windy episodes in Iceland, forest decline in western Mediterranean region, relatively drier condition in Cuba, enhanced primary productivity in the Cariaco basin (associated with a southern migration of the Atlantic ITCZ), increased rainfalls and wetter environment on the South American Altiplano, cooling events in the Southern Ocean (South Georgia), lower lake salinity in Southeastern Australia, more or dominant El-Nino-like tropical Pacific conditions and weaker East Asian monsoons (Bray, 1968, 1971, 1972; Johnsen et al., 1972; Denton and Karlen, 1973; Naidu and Malmgren, 1995; O'Brien et al., 1995; Stuiver et al., 1995; Thompson et al., 1995; Sirocko et al., 1996; Mayewski et al., 1997; Campbell et al., 1998; Thompson et al., 1998; Bianchi and McCave, 1999; Chapman and Shackleton, 2000; deMenocal et al., 2000; Giraudeau et al., 2000; Jian et al., 2000; Sarkar et al., 2000; Arz et al., 2001; Bond et al., 2001[6]; McDermott et al., 2001; Moy et al.,

---

[5] Once again, we restrict our first study to the Holocene but it is not uncommon to find the millennial-scale variability in other geological epochs. For example, the "1500-year"-like oscillations (distinct from the 1000-year and Hallstattzeit periods) have been found in the Late Miocene lake sedimentary records in South-eastern Europe by Kern et al. (2012). Franco et al. (2012) detected clear millennial-scale climatic cycles during the Permian–Carboniferous era from two glaciogenic rhythmites from the Parana basin, southeastern Brazil. Jin and Jian (2013) presented an even more exciting evidence for the existence and persistence of the 2.2 kyr, 1.6 kyr and 1.4 kyr peaks and the 2.4 kyr, 2.1 kyr, 1.7 kyr, 1.4 kyr and 1.3 kyr peaks in their $\delta^{18}O_{G,ruber}$ and Mg/Ca-derived SST records from ODP Site 1144 in the northern South China Sea during the mid-Pleistocene transition period. Such new evidence adds further motivation to clarify the true physical nature of the millennial-scale climate variation which apparently operated rather consistently regardless of the background environmental, climatic and geological conditions.

[6] It is important to point out that studies of sediments from various locations around Iceland shelf by Andrews (2009) and Andrews et al. (2009) did not yield similar drift ice proxy records to the results presented by Bond et al. (2001) from the VM129-191 core west of Ireland.

2002; Fleitmann et al., 2003; Hu et al., 2003; Marchitto and deMenocal, 2003; Risebrobakken et al., 2003; Rosqvist and Schuber, 2003; Kim et al., 2004; Moros et al., 2004; Nielsen et al., 2004; Stott et al., 2004; Baker et al., 2005; Gupta et al., 2005; Jackson et al., 2005; Turney et al., 2005; Yu et al., 2006; Asmerom et al., 2007; Crosta et al., 2007; Selvaraj et al., 2007; Thamban et al., 2007; Ekdahl et al., 2008; Goni et al., 2009; Isono et al., 2009; Moros et al., 2009; Thornalley et al., 2009; Giraudeau et al., 2010; Helama et al., 2010; Marchitto et al., 2010; Pena et al., 2010; Selvaraj et al., 2011; Strikis et al., 2011; Cleroux et al., 2012; Darby et al., 2012; Kemp et al., 2012; Schmidt et al., 2012; Sorrel et al., 2012; Fensterer et al., 2013; Fletcher et al., 2013; Kravchinsky et al., 2013; Santos et al., 2013; Wilkins et al., 2013; Zhao et al., 2013). This is an impressive range of empirical evidence, the existence of which leaves no room to doubt as to the reality of a 1500-yr or 1800-yr solar-related, though not necessarily directly solar-forced, cycle.

Perhaps even more remarkable is the strong historical and archaeo-logical evidence for the repetitive occurrences of a 500-yr long "Little Ice Ages" every 1300-yr or so over the Holocene as pointed out in Perry and Hsu (2000). Human history and civilization had apparently experienced adversities and hardships during cold and dry intervals every 1800-yr or so. As an independent test of Perry and Hsu (2000)'s hypothesis, Dixit et al. (in press) recently pointed to a clear evidence for an abrupt weakening of the Indian summer monsoon around 4100 yr BP from their study around the paleolake Kolta Dahar, Haryana, Northwest India. A prolonged monsoonal drought event between 4.6–3.6 ka BP, marked by the presence of evaporative gaylussite, has also been found in Lonar Lake, Central India (Prasad et al., 2014). This event fits well with the event "K" in Perry and Hsu (2000) where they noted that "[g]lobal cooling started as early as 4400 BP and ended some 600 years later. Archaeological evidence indicate that the years 4200–3900 BP were coldest and most arid in western Asia." (p. 12436).

It has been clear for some time that the empirical correlation on cen-tennial and millennial scales between weak solar forcing and various cold-related climatic phenomena worldwide may not be accidental. The physical relationships involved may include the application of weak solar forcing at the ocean surface and the intensity of Atlantic deep-water formation in response. This is because actively convecting, downwelling cold perturbations will communicate any near-surface anomaly to deeper North Atlantic intermediate waters much more ef-fectively than a warm (buoyant) surface anomaly can (see, e.g. the the-oretical study by Xie and Vallis, 2012). In contrast, an anomalous perturbation in warm surface water will mostly be limited and commu-nicated by much slower diffusive transport processes. It is perhaps also relevant that 1500-year is roughly equivalent to the time constant for global ocean turn-over circulation, which may physically cause a near-resonant oceanic response to external solar pacing and modulation, no matter how weak the original 1500-yr scale solar forcing variation might be.

In addition to the 1500-yr cycle, good empirical evidence exists also for solar modulation of climate-related events on multidecadal, centen-nial and bicentennial timescales (Soon, 2009; Soon et al., 2011; van Loon et al., 2012; Weng, 2012a,b; Soon and Legates, 2013). This modu-lation is manifest in variations in the equator-to-pole (Arctic) tempera-ture gradient, the surface temperature in the Arctic, the Arctic-North Atlantic freshwater budget and the Atlantic THC/MOC. In addition, re-motely teleconnected impacts on these timescales have been shown to occur in the surface temperature (Wang et al., 2009; Soon et al., 2011) and precipitation (Wang et al., 2009) in China and the East Asia region. Although computer climate/ocean modeling is only in its early stage for such solar-climatic variations, it is encouraging to see two re-cent results reporting on the penetration of the externally-forced signals on 60–90-yr and 200-yr timescales deep into not only the North Atlantic deepwater region (at about 2000 m depth) but also other parts of the inter-connected world oceans (Park and Latif, 2012; Seidenglanz et al.,

2012), as may be indicated also by some paleoceanographic observa-tions (e.g. Morley et al., 2011).

However, whether and how these various physical variations might be scaled-up to fit the 1500-year quasi-regular climatic cycles remains unclear. On the other hand, and so far confined to the admittedly ideal-ized analogy world of electronic signals interaction and processing, several careful analyses (Damon and Jirikowic, 1992; Vasiliev and Dergachev, 2002; Peristykh and Damon, 2003) have shown direct evidence for the modulation of the Gleissberg–Yoshimura cycle ampli-tude by the longer Hallstattzeit in time domain. The Hallstattzeit ~2400-yr cycle is also found as a clustering of the grand minima of solar activity (Usoskin et al., 2007). Clemens (2005) proposed that the broad peak at ~1470-yr identified in the GISP2 $\delta^{18}O$ record related to Dansgaard–Oeschger events consists instead of three narrower peaks centered around 1190-, 1490- and 1667-yr periods and that these millennial-scale periods may be explained by the beating phenomena (heterodynes) among the solar-derived centennial-scale cycles seen in Holocene record of ^{14}C production time series. This is why it is not en-tirely trivial to presume that all the identified multidecadal, centennial to millennial timescales are unrelated or simply independent oscilla-tions (see also Markonis and Koutsoyiannis, 2013).

More empirical support for a 1500-yr solar modulation of climatic events throughout the Holocene occurs in the persistent millennial, bi-millennial or 1500-yr-signals that have been recorded from many re-gions despite the dramatic changes in external boundary conditions that occurred during the Holocene. For example, in regions adjacent to former ice-caps glacioisostatic rebound has caused local relative sea-level to vary by more than 50 m between the early and late Holocene, with corresponding variations in extremes in winter-summer insolation contrast (Mayewski et al., 2004; Wanner et al., 2008).[7]

An early example of dramatic changes in intermediate water flow through the Holocene was documented by Bianchi and McCave (1999). These authors showed that the temperature and flow rate of Iceland–Scotland Overflow Water (ISOW) relationship switched from the original mode of a warm climate with slower ISOW flow rate during the early Holocene to the second mode of a faster ISOW flow rate, and hence more North Atlantic deep water formation, during the warmer conditions that pertained in Greenland and Northern Europe after about 7.5 kyr BP. Supporting this, Dima and Lohmann (2009; their Fig. 6d) showed that the 1400-yr variation was relatively muted from 10–7.5 kyr BP, after which it oscillated at larger amplitudes during the middle to late Holocene. The proxy record of forest vegetation from western Mediterranean marine core MD95-2043 shows a strong 900-yr scale variation during the early Holocene and a switch into the dom-inant 1750-yr periodicity after 6 kyr BP (Fletcher et al., 2013). Another example is the persistent millennial-scale signal that appears through-out the Holocene in lacustrine $\delta^{18}O$ and $\delta^{13}C$ sediment records from Lake Grinnell, northern New Jersey (910-yr periodicity, as identified in Zhao et al., 2010). As these authors point out, their data imply a nonlin-ear response in atmospheric circulation during the Holocene. A possible causal chain is that a decreased winter-summer seasonal contrast in in-solation led to the observed transition between a large-amplitude 330-yr oscillation and a low-amplitude 500-yr oscillation in the mid-Holocene (ca. 4.7 kyr BP). Such a nonlinear switch in conditions is con-sistent with a switch between the fundamental and derived climatic modes hypothesized by Dima and Lohmann (2009).

Our overall conclusion is to concur with Munk et al. (2002, p. 382) who insightfully commented that further investigations into the 1500-yr cycle should be conducted in a spirit that favors "processes with millennial time constants (not yet identified) inherent in

---

[7] This is one of the reasons why the proposition of a "stable" climate, say with a regional warming and cooling range within ± 0.5 °C, during the entire Holocene is an untenable idea that can be rejected by paleoclimatic evidence (Mayewski et al., 2004; Wanner et al., 2008).

ocean-atmosphere dynamics as the source of the millennial climate variability", and who added that "millennial variability in solar radiation (not yet discovered) is a possibility."

4. Conclusions

We have used multiple-cross wavelet analysis of three solar activity proxies and seven paleoclimate proxies to demonstrate the ubiquitous nature of both solar and climatic rhythmicities at centennial and millennial timescales throughout the Holocene. The climatic proxies used represent variation in the North Atlantic Ocean, Western Pacific Warm Pool, Southern Ocean and the East Asian monsoon regions, and alongside the conventional ^{10}Be and ^{14}C solar activity proxies we have introduced a new solar proxy that is based upon the variation of nitrate (NO_3^-) concentration in the Talos Dome ice core, East Antarctica.

Our interpretations have been greatly aided by the introduction of a novel algorithm for computing multiple-cross wavelet spectra in time–frequency space that is generalized for multiple time series (more than two).

Our results provide a new interpretive framework for relating Holocene solar activity variation on centennial to millennial timescales to co-varying climate proxies drawn from a widespread area around the globe, and include the following specific conclusions:

o Fundamental solar modes (in the sense of Dima and Lohmann, 2009) exist at 2300-yr (Hallstattzeit), 1000-yr (Eddy), and 500-yr (unnamed) periodicities.
o Dating uncertainties allow that the commonly remarked 1500-yr and 1800-yr cycles, which are also present in our wavelet analysis, may represent either the same or discrete cyclicities. Nonetheless, the TALDICE nitrate record clearly identifies the 1500-yr signal (Fig. 2), while the cross-wavelet analysis of the three solar activity proxies show a strongly modulated and time-dependent signal for the 1800-yr (blue line at the bottom panel of Fig. 3).
o Thus an important implication of our study is that the widely observed 1500–1800-yr oscillation may yet turn out to correspond to a fundamental solar mode. The suggestion by Dima and Lohmann (2009) that the 1500–1800-yr cycle is of derived rather than fundamental character, and the rejection of the 1500–1800-yr scale as a solar-originated oscillation at all (Debret et al., 2009; Darby et al., 2012; Obrochta et al., 2012; Sorrel et al., 2012), are therefore both premature.
o Nonetheless, it remains possible that the 1500–1800-yr cycle is indeed distinct in character from the fundamental solar cycles that we describe and instead represents an internal threshold response of the global thermohaline circulation to solar forcing, and is therefore of derived nature, all as argued by Dima and Lohmann (2009). Similarly, intermediary cycles that our analysis identifies at 700-yr and 300-yr periodicities may also be of derived nature, and perhaps mark the rectified responses of the Atlantic thermohaline circulation to external solar modulation and pacing.

We conclude that is premature to reject possible links between solar activity and terrestrial climate at the multiple scales that are commonly represented in paleoclimatic records. Instead, we find that strong empirical evidence supports the existence of sun–climate relationships on a number of centennial-to-millennial, suborbital timescales, and that these relationships are represented by climate proxy variations from nearly all the Earth's major climatic zones and regimes.

This broad conclusion needs clarification in terms of both the physical nature of the solar variability and of the precise mechanisms that are involved in the manifestation of solar changes in variable and varying local and regional climate patterns. *Inter alia*, knowledge is needed as to how different climatic regions may respond to solar changes at different time scales, including knowledge of the physical processes that are related to the high polar regions, the North Atlantic MOC and the tropical coupled ocean–atmosphere deep convection and ENSO phenomena. It is also yet to be established whether a dominant climatic center-of-action exists (i.e., polar, mid-latitude or tropical) that dominates the global climatic pattern.

Identifying and understanding the spatial–temporal relationships between solar variability and climatic response may well be aided by the application of our new cross-wavelet algorithm to additional and new high resolution paleoclimate proxy records.

Appendix A. A new algorithm for multiple-cross-wavelet analysis with multiple time series

The generalized multiple-cross-wavelet transform algorithm to study coherent variations in multiple (>2) time series is briefly described. The cross function is a technique for measuring the similarity of one signal to another and was proposed by Wiener (1930).

Our algorithm is the generalization of the Wiener's (1930) cross function, but instead of considering the functions F and G, we consider two matrices $F(t)$ and $G(t)$ in which each of its elements are the time-dependent functions itself:

$$F(t) = \begin{bmatrix} F_1 \\ F_2 \\ F_3 \\ \vdots \\ F_n \end{bmatrix}; \quad G(t) = [G_1 G_2 G_3 \cdots G_m].$$

The wavelet of the matrices F and G is respectively:

$$W[F(t)] = W_F = \begin{bmatrix} W_{F_1} \\ W_{F_2} \\ W_{F_3} \\ \vdots \\ W_{F_n} \end{bmatrix}; \quad W[G(t)]^* = W_G^*$$

$$= \begin{bmatrix} W_{G_1}^* & W_{G_2}^* & W_{G_3}^* & \dots & W_{G_m}^* \end{bmatrix}.$$

The hyper cross-matrix wavelet is defined as:

$$W_F W_G^* = W_{FG} = \begin{bmatrix} W_{F_1 G_1} & W_{F_1 G_2} & W_{F_1 G_3} & \cdots W_{F_1 G_m} \\ W_{F_2 G_1} & W_{F_2 G_2} & W_{F_1 G_3} & \cdots W_{F_1 G_1} \\ \vdots & \vdots & \vdots & \ddots & \vdots \\ W_{F_n G_1} & W_{F_n G_2} & W_{F_n G_3} & \cdots W_{F_n G_m} \end{bmatrix}$$

where each element of the hyper cross-matrix are one cross wavelet matrix:

$$W_{F_iG_k}(s) = W_{F_i}(s)W^*_{G_k}(s).$$

We next define the multiple cross wavelets as:

$$W_{F_iG_k} = \left\langle W_{F_i}\prod_{k=1}^{n} W^*_{G_k}\right\rangle$$

where $\langle\cdot\rangle$ indicates an average of the multiple cross wavelets and Π means multiplication.

The phase angle of $W^{X_1,X_2,X_3,\ldots,X_m}$ describes the phase relationship between the $X_1, X_2, X_3,\ldots,X_m$ series in time–frequency space. Statistical significance of the multiple-cross-wavelet coherence is estimated using Monte Carlo methods with red noise to determine the 5% significance level (Torrence and Webster, 1999).

The panels on the right of Figs. 3 and 4 show the global phase information, which is an average phase angle of each periodicity in the multiple-cross-wavelet spectra. The bottom panels in Fig. 3 and 4 give the instantaneous phase and amplitude for the selected millennial-scale oscillatory scale of 1885-years. Therefore, these panels provide information on the lead–lag relationship of the time series involved.

In order to test and illustrate the accuracy and correctness of our new multiple-cross-wavelet for multiple time series, we offer the following two contrasting examples:

(1) analyzes the multiple-cross wavelet transform spectrum for the following 3 time series
  (a) cos (10 t)
  (b) cos (10 t) + cos (50 t)
  (c) cos (10 t) + cos (50 t) + cos (100 t)
(2) analyzes the multiple-cross wavelet transform spectrum for the following 3 time series
  (a) cos (10 t)
  (b) cos (50 t)
  (c) cos (50 t) + cos (100 t)

where for former is intended for finding a common scale of 10 time units and the later is intended to yield no common scale for the three time series.

Fig. A1 confirms this fact and hence the feasibility of our new algorithm for time series analysis of real data records. Fig. A1 also confirms that in order for the algorithm to identify a true common signal, it is not sufficient to have only two out of three of the time series to have
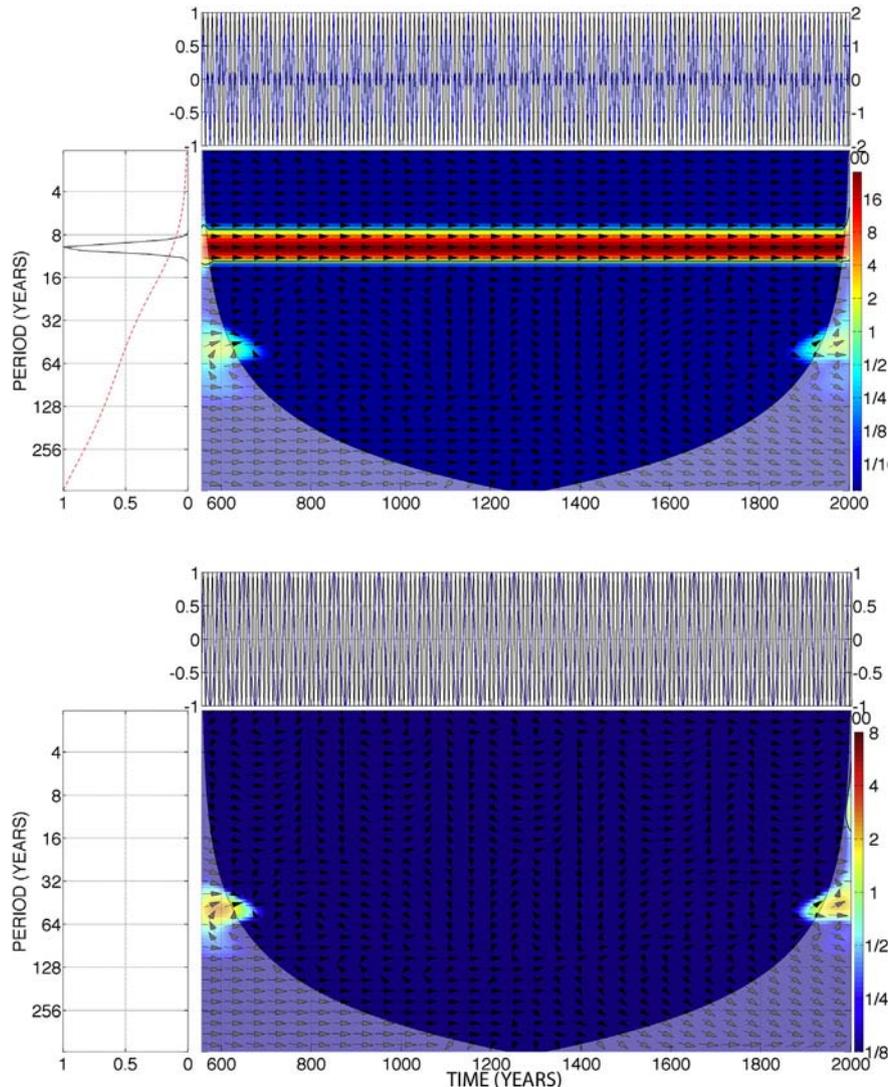

Fig. A1. (Top) Cross wavelet analysis for the 3 idealized time series: cos (10 t), cos (10 t) + cos (50 t) and cos (10 t) + cos (50 t) + cos (100 t). A common periodicity is successfully detected at 10 time units. (Bottom) Cross wavelet analysis for the 3 idealized time series: cos (10 t), cos (50 t) and cos (50 t) + cos (100 t). No common periodicity is found for the 3 time series.

the common scale, i.e., the 50 time units was not picked up in the final cross wavelet of the 3-time series.

Finally, we wish to explain and clarify that more details about the mathematics of our new algorithm will be fully spelled out in a future paper that focuses on methodology rather than application as intended in the current paper. Here we simply wish to state that there is simply no clear nor direct way to inter-compare this study with any previous methods (especially those based on Fourier transform) because no previous analysis has simultaneously cross-correlated information on both a time and frequency basis for multiple (>2) time series. This is the reason why we have chosen to illustrate the nature of our new algorithm with the simple example demonstrated in Fig. A1.

References

Abreu, J.A., Beer, J., Ferriz-Mas, A., McCracken, K.G., Steinhilber, F., 2012. Is there a planetary influence on solar activity? Astron. Astrophys. 548, A88.

Andrews, J.T., 2009. Seeking a Holocene drift ice proxy: non-clay mineral variations from the SW to N-central Iceland shelf: Trends, regime shifts, and periodicities. J. Quat. Sci. 24, 664–676.

Andrews, J.T., Darby, D., Eberle, D., Jennings, A.E., Moros, M., Ogilvie, A., 2009. A robust, multisite Holocene history of drift ice off northern Iceland: Implications for North Atlantic climate. The Holocene 19, 71–77.

Arz, H.W., Gerhardt, S., Patzold, J., Rohl, U., 2001. Millennial-scale changes of surface- and deep-water flow in the western tropical Atlantic linked to Northern Hemisphere high-latitude climate during the Holocene. Geology 29, 239–242.

Asmerom, Y., Polyak, V., Burns, S., Rassmussen, J., 2007. Solar forcing of Holocene climate: new insights from a speleothem record, southwestern United States. Geology 35, 1–4.

Baker, P.A., Fritz, S.C., Garland, J., Ekdahl, E., 2005. Holocene hydrologic variation at Lake Titicaca, Bolivia/Peru, and its relationship to North Atlantic climate variation. J. Quat. Sci. 20, 655–662.

Berger, A., Loutre, M.E., 1991. Insolation values for the climate of the last 10 million years. Quat. Sci. Rev. 10, 297–317.

Bianchi, G.G., McCave, I.N., 1999. Holocene periodicity in North Atlantic climate and deep-ocean flow south of Iceland. Nature 397, 515–517.

Bond, G., Kromer, B., Beer, J., Muscheler, R., Evans, M.N., Showers, W., Hoffmann, S., Lotti-Bond, R., Hajdas, I., Bonani, G., 2001. Persistent solar influence on North Atlantic climate during the Holocene. Science 294, 2130–2136.

Brandenburg, A., Spiegel, E.A., 2008. Modeling a Maunder minimum. Astron. Nachr. 329, 351–358.

Bray, J.R., 1968. Glaciation and solar activity since the fifth century BC and the solar cycle. Nature 220, 672–674.

Bray, J.R., 1971. Solar-climate relationships in the post-Pleistocene. Science 171, 1242–1243.

Bray, J.R., 1972. Cyclic temperature oscillations from 0–20,300 yr BP. Nature 237, 277–279.

Campbell, I.D., Campbell, C., Apps, M.J., Rutter, N.W., Bush, A.B.G., 1998. Late Holocene 1500 yr climatic periodicities and their implications. Geology 26, 471–473.

Chapman, M.R., Shackleton, N.J., 2000. Evidence of 550-year and 1000-year cyclicities in North Atlantic circulation patterns during the Holocene. The Holocene 10, 287–291.

Clemens, S.C., 2005. Millennial-band climate spectrum resolved and linked to centennial-scale solar cycles. Quat. Sci. Rev. 24, 521–531.

Cleroux, C., Debret, M., Cortijio, E., Duplessy, J.-C., Dewilde, F., Reijmer, J., Massei, N., 2012. High-resolution sea surface reconstructions off Cape Hatteras over the last 10 ka. Paleoceanography 27. http://dx.doi.org/10.1029/2011PA002184.

Crosta, X., Debret, M., Denis, D., Courty, M.A., Ther, O., 2007. Holocene long- and short-term climate changes off Adelie Land, East Antarctica. Geochem. Geophys. Geosyst. 8. http://dx.doi.org/10.1029/2007GC001718.

Damon, P.E., Jirikowic, J.L., 1992. The Sun as a low-frequency harmonic oscillator. Radiocarbon 34, 199–205.

Darby, D.A., Ortiz, J.D., Grosch, C.E., Lund, S.P., 2012. 1,500-year cycle in the Arctic Oscillation identified in Holocene Arctic sea-ice drift. Nat. Geosci. 5, 897–900. http://dx.doi.org/10.1038/NGEO1629.

de Rop, W., 1971. A tidal period of 1800 years. Tellus 23, 261–262.

Debret, M., Bout-Roumazeilles, V., Grousset, F., Desmet, M., McManus, J.F., Massei, N., Sebag, D., Petit, J.-R., Copard, Y., Trentesaux, A., 2007. The origin of the 1500-year climate cycles in Holocene North-Atlantic records. Clim. Past 3, 569–575.

Debret, M., Sebag, D., Crosta, X., Massei, N., Petit, J.-R., Chapron, E., Bout-Roumazeilles, V., 2009. Evidence from wavelet analysis for a mid-Holocene transition in a global climate forcing. Quat. Sci. Rev. 28, 2675–2688.

deMenocal, P., Ortiz, J., Guilderson, T., Sarnthein, M., 2000. Coherent high- and low-latitude climate variability during the Holocene warm period. Science 288, 2198–2202.

Denton, G.H., Broecker, W.S., 2008. Wobbly ocean conveyor circulation during the Holocene? Quat. Sci. Rev. 27, 1939–1950.

Denton, G.H., Karlen, W., 1973. Holocene climatic variations—their pattern and possible cause. Quat. Res. 3, 155–205.

Dima, M., Lohmann, G., 2009. Conceptual model for millennial climate variability: a possible combined solar-thermohaline circulation origin for the 1500-year cycle. Clim. Dyn. 32, 301–311.

Ditlevsen, P.D., Kristensen, M.S., Andersen, K.K., 2005. The recurrence time of Dansgaard–Oeschger events and limits on the possible periodic component. J. Clim. 18, 2594–2603.

Ditlevsen, P.D., Andersen, K.K., Svensson, A., 2007. The DO-climate events are probably noise induced: statistical investigation of the claimed 1470 years cycle. Clim. Past 3, 129–134.

Dixit, Y., Hodell, D.A., Petrie, C.A., 2014. Abrupt weakening of the summer monsoon in northwest India 4100 yr ago. Geology. http://dx.doi.org/10.1130/G35236.1 (in press).

Ekdahl, E.J., Fritz, S.C., Baker, P.A., Rigsby, C.A., Coley, K., 2008. Holocene multidecadal-to millennial-scale hydrologic variability on the South American Altiplano. The Holocene 18, 867–876.

Essex, C., 2011. Climate theory versus a theory for climate. Int. J. Bifurcation Chaos 21, 3477–3487.

Essex, C., 2013. Does laboratory-scale physics obstruct the development of a theory for climate? J. Geophys. Res. 118. http://dx.doi.org/10.1029/jgrd.50195.

Farge, M., 1992. Wavelet transforms and their applications to turbulence. Annu. Rev. Fluid Mech. 24, 395–457.

Fensterer, C., Scholz, D., Hoffmann, D.L., Spotl, C., Schroder-Ritzrau, A., Horn, C., Pajon, J.M., Mangini, A., 2013. Millennial-scale climate variability during the last 12.5 ka recorded in a Caribbean speleothem. Earth Planet. Sci. Lett. 361, 143–151.

Fleitmann, D., Burns, S.J., Mudelsee, M., Neff, U., Kramers, J., Mangini, A., Matter, A., 2003. Holocene forcing of the Indian monsoon recorded in a stalagmite from Southern Oman. Science 300, 1737–1739.

Fletcher, W.J., Debret, M., Sanche Goni, M.F., 2013. Mid-Holocene emergence of a low-frequency millennial oscillation in western Mediterranean climate: implications for past dynamics of the North Atlantic atmospheric westerlies. The Holocene 23, 153–166. http://dx.doi.org/10.1177/0959683612460783.

Franco, D.R., Hinnov, L.A., Ernesto, M., 2012. Millennial-scale climate cycles in Permian-Carboniferous rhythmites: permanent feature throughout geologic time? Geology 40, 19–22.

Frick, P., Baliunas, S., Galyagin, D., Sokoloff, Soon, W., 1997. Wavelet analysis of stellar chromospheric activity variations. Astrophys. J. 483, 426–434.

Giraudeau, J., Cremer, M., Manthe, S., Labeyrie, L., Bond, G., 2000. Coccolith evidence for instabilities in surface circulation south of Iceland during Holocene times. Earth Planet. Sci. Lett. 179, 257–268.

Giraudeau, J., Grelaud, M., Solignac, S., Andrews, J.T., Moros, M., Jansen, E., 2010. Millennial-scale variability in Atlantic water advection to the Nordic Seas derived from Holocene coccolith concentration records. Quat. Sci. Rev. 29, 1276–1287.

Goni, M.A., Aceves, H., Benitez-Nelson, B., Tappa, E., Thunell, R., Black, D.E., Muller-Karger, F., Astror, Y., Valera, R., 2009. Oceanographic and climatologic controls on the compositions and fluxes of biogenic materials in the water column and sediments of the Carico Basin over the late Holocene. Deep Sea Res. I 56, 614–640.

Gough, D.O., 1990. On possible origins of relatively short-term variations in the solar structure. Philos. Trans. R. Soc. Lond. A330, 627–640.

Gough, D.O., 2002. How is solar activity influencing the structure of the Sun? From Solar Min to Max: Half a Solar Cycle with SOHO, Proceedings of SOHO 11 Symposium, (European Space Agency SP-508), pp. 577–592.

Gupta, A.K., Anderson, D.M., Overpeck, J.T., 2003. Abrupt changes in the Asian southwest monsoon during the Holocene and their links to the North Atlantic Ocean. Nature 421, 354–357.

Gupta, A.K., Das, M., Anderson, D.M., 2005. Solar influence on the Indian summer monsoon during the Holocene. Geophys. Res. Lett. 32. http://dx.doi.org/10.1029/2005GL022685.

Hanslmeier, A., Brajsa, R., Calogovic, J., Vrsnak, B., Ruzdjak, D., Steinhilber, F., MacLeod, C.L., Ivezic, Z., Skokic, Z.H., 2013. The chaotic solar cycle II. Analysis of cosmogenic 10Be data. Astron. Astrophys. 550, A6.

Helama, S., Fauria, M.M., Mielikainen, K., Timonen, M., Eronen, M., 2010. Sub-Milankovitch solar forcing of past climates: mid and late Holocene perspectives. Geol. Soc. Am. Bull. 122, 1981–1988.

Hu, F.S., Kaufman, D., Yoneji, S., Nelson, D., Shemesh, A., Huang, Y., Tian, J., Bond, G., Clegg, B., Brown, T., 2003. Cyclic variation and solar forcing of Holocene climate in the Alaskan subarctic. Science 301, 1890–1893.

Hudgins, L., Friehe, C.A., Mayer, M.E., 1993. Wavelet transforms and atmospheric turbulence. Phys. Rev. Lett. 71, 3279–3282.

Isono, D., Yamamoto, M., Irino, T., Oba, T., Murayama, M., Nakamura, T., Kawahata, H., 2009. The 1500-year climate oscillation in the midlatitude North Pacific during the Holocene. Geology 37, 591–594.

Jackson, M.G., Oskarsson, N., Tronnes, R.G., McManus, J.F., Oppo, D.W., Gronvold, K., Hart, S.R., Sachs, J.P., 2005. Holocene loess deposition in Iceland: evidence for millennial scale atmosphere–ocean coupling in the North Atlantic. Geology 33, 509–512.

Jian, Z., Wang, P., Saito, Y., Wang, J., Pflaumann, U., Oba, T., Cheng, X., 2000. Holocene variability of the Kuroshio Current in the Okinawa Trough, northwestern Pacific Ocean. Earth Planet. Sci. Lett. 184, 305–319.

Jin, H., Jian, Z., 2013. Millennial-scale climate variability during the mid-Pleistocene transition period in the northern South China Sea. Quat. Sci. Rev. 70, 15–27.

Johnsen, S.J., Dansgaard, W., Clausen, H.B., Langway, C.C., 1972. Oxygen isotope profiles through the Antarctic and Greenland ice sheets. Nature 235, 429–434.

Kanda, S., 1933. Ancient records of sunspots and auroras in the Far East and the variation of the period of solar activity. Proc. Imp. Acad. 9, 293–296.

Kao, S.J., Horng, C.S., Hsu, S.C., Wei, K.Y., Chen, J., Lin, Y.S., 2005. Enhanced deepwater circulation and shift of sedimentary organic matter oxidation pathway in the Okinawa Trough since the Holocene. Geophys. Res. Lett. 32, L15609. http://dx.doi.org/10.1029/2005GL023139.

Keeling, C.D., Whorf, T.P., 2000. The 1800-year oceanic tidal cycle: a possible cause of rapid climate change. Proc. Natl. Acad. Sci. U. S. A. 97, 3814–3819.

Kemp, J., Radke, L.C., Olley, J., Juggins, S., de Deckker, P., 2012. Holocene lake salinity changes in the Wimmera, southeastern Australia, provide evidence for millennial-scale climate variability. Quat. Res. 77, 65–76.

Kern, A.K., Harzhauser, M., Piller, W.E., Mandic, O., Soliman, A., 2012. Strong evidence for the influence of solar cycles on a Late Miocene lake system revealed by biotic and abiotic proxies. Palaeogeogr. Palaeoclimatol. Palaeoecol. 329–330, 124–136.

Kim, J.-H., Rimbu, N., Lorenz, S.J., Lohmann, G., Nam, S.-I., Schouten, S., Ruhlemann, C., Schneider, R.R., 2004. North Pacific and North Atlantic sea-surface temperature variability during the Holocene. Quat. Sci. Rev. 23, 2141–2154.

Konecky, B.L., Russell, J.M., Rodysill, J.R., Vuille, M., Bijaksana, S., Huang, Y., 2013. Intensification of southwestern Indonesian rainfall over the past millennium. Geophys. Res. Lett. 40, 386–391. http://dx.doi.org/10.1029/2012GL054331.

Kravchinsky, V.A., Langereis, C.G., Walker, S.D., Dlusskiy, K.G., White, D., 2013. Discovery of Holocene millennial climate cycles in the Asian continental interior: has the sun been governing the continental climate? Global Planet. Change 110, 386–396. http://dx.doi.org/10.1016/j.gloplacha.2013.02.011.

Laluraj, C.M., Thamban, M., Naik, S.S., Redkar, B.L., Chaturvedi, A., Ravindra, R., 2011. Nitrate records of a shallow ice core from East Antarctica: atmospheric processes, preservation and climatic implications. The Holocene 21, 351–356.

Lim, J., Yi, S., Nahm, W.-H., Kim, J.-Y., 2012. Holocene millennial-scale vegetation changes in the Yugu floodplain, Kongju area, central South Korea. Quat. Int. 254, 92–98.

Lim, J., Nahm, W.-H., Kim, J.-Y., Yang, D.-Y., 2013. Reply to comment on "" by J. Lim, W.-H., Nahm, J.-K., Kim, D.-Y., Yang [Palaeogeography, Palaeoclimatology, Palaeoecology 298 (2010) 370–377]. Palaeogeogr. Palaeoclimatol. Palaeoecol. 392, 559–561. http://dx.doi.org/10.1016/j.palaeo.2013.08.004.

Lou, J.Y., Chen, C.T.A., 1997. Paleoclimatological and paleoenvironmental records since 4000 a B.P. in the sediments of alpine lakes in Taiwan. Sci. China D Earth Sci. 40, 424–431.

Mackay, A.W., Swann, G.E.A., Fagel, N., Fietz, S., Leng, M.J., Morley, D., Rioual, P., Tarasov, P., 2013. Hydrological instability during the Last Interglacial in central Asia: a new diatom oxygen isotope record from Lake Baikal. Quat. Sci. Rev. 66, 45–54.

Marchitto, T.M., deMenocal, P.B., 2003. Late Holocene variability of upper North Atlantic deep water temperature and salinity. Geochem. Geophys. Geosyst. 4. http://dx.doi.org/10.1029/2003GC000598.

Marchitto, T.M., Muscheler, R., Ortiz, J.D., Carriquiry, J.D., van Geen, A., 2010. Dynamical response of the tropical Pacific Ocean to solar forcing during the early Holocene. Science 330, 1378–1381.

Markonis, Y., Koutsoyiannis, D., 2013. Climatic variability over time scales spanning nine orders of magnitude: connecting Milankovitch cycles with Hurst–Kolmogorov dynamics. Surv. Geophys. 34, 181–207. http://dx.doi.org/10.1007/s10712-012-9208-9.

Mayewski, P.A., Meeker, L.D., Twickler, M.S., Whitlow, S., Yang, Q., Lyons, W.B., Prentice, M., 1997. Major features and forcing of high-latitude northern hemisphere atmospheric circulation using a 110,000-year-long glaciochemical series. J. Geophys. Res. 102, 26345–26366. http://dx.doi.org/10.1029/96JC03365.

Mayewski, P.A., Rohling, E.E., Stager, J.C., Karlen, W., Maasch, K.A., Meeker, L.D., Meyerson, E.A., Gasse, F., van Kreveld, S., Holmgren, K., Lee-Thorp, J., Rosqvist, G., Rack, F., Staubwasser, M., Schneider, R.R., Steig, E.J., 2004. Holocene climatic variability. Quat. Res. 62, 243–255.

McCracken, K.G., Dreschhoff, G.A.M., Zeller, E.J., Smart, D.F., Shea, M.A., 2001. Solar cosmic ray events for the period 1561–994: 1. Identification in polar ice, 1561–1950. J. Geophys. Res. 106. http://dx.doi.org/10.1029/2000JA000237.

McDermott, F., Mattey, D.P., Hawkesworth, C., 2001. Centennial-scale Holocene climate variability revealed by a high-resolution speleothem δ^{18}O record from SW Ireland. Science 294, 1328–1331 ([with erratum printed 16 September 2005]).

Morley, A., Schulz, M., Rosenthal, Y., Mulitza, S., Paul, A., Ruhlemann, C., 2011. Solar modulation of North Atlantic central water formation at multidecadal timescales during the late Holocene. Earth Planet. Sci. Lett. 308, 161–171.

Moros, M., Emeis, K., Risebrobakken, B., Snowball, I., Kuijpers, A., McManus, J., Jansen, E., 2004. Sea surface temperatures and ice rafting in the Holocene North Atlantic: climate influences on northern Europe and Greenland. Quat. Sci. Rev. 23, 2113–2126.

Moros, M., Deckker, P.D., Jansen, E., Perner, K., Telford, R.J., 2009. Holocene climate variability in the Southern Ocean recorded in a deep-sea sediment core off South Australia. Quat. Sci. Rev. 28, 1932–1940.

Moy, C.M., Seltzer, G.O., Rodbell, D.T., Anderson, D.M., 2002. Variability of El Nino/Southern Oscillation activity at millennial timescales during the Holocene epoch. Nature 420, 162–165.

Munk, W., Dzieciuch, M., Jayne, S., 2002. Millennial climate variability: is there a tidal connection? J. Clim. 15, 370–385.

Naidu, P.D., Malmgren, B.A., 1995. A 2,200 years periodicity in the Asian monsoon system. Geophys. Res. Lett. 22, 2361–2364. http://dx.doi.org/10.1029/95GL02558.

Nielsen, S.H.H., Koc, N., Crosta, X., 2004. Holocene climate in the Atlantic sector of the Southern Ocean controlled by insolation or oceanic circulation? Geology 32, 317–320.

Noren, A.J., Bierman, P.R., Steig, E.J., Lini, A., Southon, J., 2002. Millennial-scale storminess variability in the northeastern United States during the Holocene epoch. Nature 419, 821–824.

O'Brien, S.R., Mayewski, P.A., Meeker, L.D., Meese, D.A., Twickler, M.S., Whitlow, S.I., 1995. Complexity of Holocene climate as reconstructed from a Greenland ice core. Science 270, 1962–1964.

Obrochta, S.P., Miyahara, H., Yokoyama, Y., Crowley, T.J., 2012. A re-examination of evidence for the North Atlantic "1500-year cycle" at Site 609. Quat. Sci. Rev. 55, 23–33.

Ogurtsov, M.G., Oinonen, M., 2014. Evidence of the solar Gleissberg cycle in the nitrate concentration in polar ice. J. Atmos. Sol. Terr. Phys. 109, 37–42.

Panovska, S., Finlay, C.C., Hirt, A.M., 2013. Observed periodicities and the spectrum of field variations in Holocene magnetic records. Earth Planet. Sci. Lett. 373, 88–94.

Park, W., Latif, M., 2012. Atlantic meridional overturning circulation response to idealized external forcing. Clim. Dyn. 39, 1709–1726.

Pena, L.D., Frances, G., Diz, P., Esparza, M., Grimalt, J.O., Nombela, M.A., Alejo, I., 2010. Climate fluctuations during the Holocene in NW Iberia: High and low latitude linkages. Cont. Shelf Res. 30, 1487–1496.

Peristykh, A.N., Damon, P.E., 2003. Persistence of the Gleissberg 88-year solar cycle over the last 12,000 years: evidence from cosmogenic isotopes. J. Geophys. Res. 108. http://dx.doi.org/10.1029/2002JA009390.

Perry, C.A., Hsu, K.J., 2000. Geophysical, archaeological, and historical evidence support a solar-output model for climate change. Proc. Natl. Acad. Sci. U. S. A. 97, 12433–12438.

Petersen, S.V., Schrag, D.P., Clark, P.U., 2013. A new mechanism for Dansgaard–Oeschger cycles. Paleoceanography 28, 24–30. http://dx.doi.org/10.1029/2012PA002364.

Pipin, V.V., 1999. The Gleissberg cycle by a nonlinear αΛ dynamo. Astron. Astrophys. 346, 295–302.

Pipin, V.V., Sokoloff, D.D., Usoskin, I.G., 2012. Variations of the solar cycle profile in a solar dynamo with fluctuating dynamo governing parameters. Astron. Astrophys. 542, A26.

Pipin, V.V., Sokoloff, D.D., Usoskin, I.G., 2013. Waldmeier relations and the solar cycle dynamics by the mean-field dynamos. In: Kosovichev, A.G., de Gouveia Dal Pinto, E.M., Yan, Y. (Eds.), Solar and Astrophysical Dynamos and Magnetic Activity (IAU Symposium No. 294) ([available at http://arxiv.org/abs/1211.2423]).

Pisias, N.G., Clark, P.U., Brook, E.J., 2010. Modes of global climate variability during Marine Isotope Stage 3 (60–26 ka). J. Clim. 23, 1581–1588.

Prasad, S., Anoop, A., Riedel, N., Sarkar, S., Menzel, P., Basavaiah, N., Krishnan, R., Fuller, D., Plessen, B., Gaye, B., Rohl, U., Wilkes, H., Sachse, D., Sawant, R., Wiesner, M.G., Stebich, M., 2014. Prolonged monsoon droughts and links to Indo-Pacific warm pool: a Holocene record from Lonar Lake, central India. Earth Planet. Sci. Lett. 391, 171–182.

Risebrobakken, B., Jansen, E., Anderson, C., Mjelde, E., Hevroy, K., 2003. Solar forcing of Florida Straits surface salinity during the early Holocene. Paleoceanography 18. http://dx.doi.org/10.1029/2002PA000764.

Rosqvist, G., Schuber, P., 2003. Millennial-scale climate changes on South Georgia, Southern Ocean. Quat. Res. 59, 470–475.

Santos, T.P., Franco, D.R., Barbosa, C.F., Belem, A.L., Dokken, T., Albuquerque, A.L.S., 2013. Millennial- to centennial-scale changes in sea surface temperature in the tropical South Atlantic throughout the Holocene. Palaeogeogr. Palaeoclimatol. Palaeoecol. 392, 1–8. http://dx.doi.org/10.1016/j.palaeo.2013.08.019.

Sarkar, A., Ramesh, R., Somayajulu, B.L.K., Agnihotri, R., Jull, A.J.T., Burr, G.S., 2000. High resolution Holocene monsoon record from the eastern Arabian Sea. Earth Planet. Sci. Lett. 177, 209–218.

Savarino, J., Kaiser, J., Morin, S., Sigman, D.M., Thiemens, M.H., 2007. Nitrogen and oxygen isotopic constraints on the origin of atmospheric nitrate in coastal Antarctica. Atmos. Chem. Phys. 7, 1925–1945.

Schmidt, M.W., Weinlein, W.A., Marcantonio, F., Lynch-Stieglitz, J., 2012. Solar forcing of Florida Straits surface salinity during the early Holocene. Paleoceanography 27. http://dx.doi.org/10.1029/2012PA002284.

Schulz, M., 2002. On the 1470-year pacing of Dansgaard–Oeschger warm events. Paleoceanography 17. http://dx.doi.org/10.1029/2000PA000571.

Schulz, M., Berger, W.H., Sarnthein, M., Grootes, P.M., 1999. Amplitude variations of 1470-year climate oscillations during the last 100,000 years linked to fluctuations of continental ice mass. Geophys. Res. Lett. 26, 3385–3388. http://dx.doi.org/10.1029/1999GL006069.

Seidenglanz, A., Prange, M., Varma, V., Schulz, M., 2012. Ocean temperature response to idealized Gleissberg and de Vries solar cycles in a comprehensive climate model. Geophys. Res. Lett. 39. http://dx.doi.org/10.1029/2012GL053624.

Selvaraj, K., Chen, C.-T.A., Lou, J.-Y., 2007. Holocene East Asian monsoon variability: links to solar and tropical Pacific forcing. Geophys. Res. Lett. 34. http://dx.doi.org/10.1029/2006GL028155.

Selvaraj, K., Chen, C.-T.A., Lou, J.-Y., Kotlia, B.S., 2011. Holocene weak summer East Asian monsoon intervals in Taiwan and plausible mechanisms. Quat. Int. 229, 57–66.

Sirocko, F., Garbe-Schonberg, D., McIntyre, A., Molfino, B., 1996. Teleconnections between subtropical monsoons and high-latitude climates during the last deglaciation. Science 272, 526–529.

Soon, W., 2009. Solar Arctic-mediated climate variation on multidecadal to centennial timescales: empirical evidence, mechanistic explanation, and testable consequences. Phys. Geogr. 30, 144–184.

Soon, W., Legates, D.R., 2013. Solar irradiance modulation of equator-to-pole (Arctic) temperature gradients: empirical evidence for climate variation on multidecadal timescales. J. Atmos. Sol. Terr. Phys. 93, 45–56.

Soon, W., Frick, P., Baliunas, S., 1999. Lifetime of surface features and stellar rotation: a wavelet time–frequency approach. Astrophys. J. Lett. 510, L135–L138.

Soon, W., Dutta, K., Legates, D.R., Velasco, V., Zhang, W., 2011. Variation in surface air temperature of China during the 20th Century. J. Atmos. Sol. Terr. Phys. 73, 2331–2344.

Sorrel, P., Debret, M., Billeaud, I., Jaccard, S.L., McManus, J.F., Tessier, B., 2012. Persistent non-solar forcing of Holocene storm dynamics in coastal sedimentary archives. Nat. Geosci. 5, 892–896. http://dx.doi.org/10.1038/NGEO1619.

Spiegel, E.A., 2009. Chaos and intermittency in the solar cycle. Space Sci. Rev. 144, 25–51.

Stenni, B., Proposito, M., Gragnani, R., Flora, O., Jouzel, J., Falourd, S., Frezzotti, M., 2002. Eight centuries of volcanic signal and climate change at Talos Dome (East Antarctica). J. Geophys. Res. 107. http://dx.doi.org/10.1029/2000JD000317.

St-Onge, G., Stoner, J.S., Hillaire-Marcel, C., 2003. Holocene paleomagnetic records from the St. Lawrence estuary, eastern Canada: Centennial- to millennial-scale geomagnetic modulation of cosmogenic isotopes. Earth Planet. Sci. Lett. 209, 113–130.

Stott, L., Cannariato, K., Thunell, R., Haug, G.H., Koutavas, A., Lund, S., 2004. Decline of surface temperature and salinity in the western tropical Pacific Ocean in the Holocene epoch. Nature 431, 56–59.

Strikis, N.M., Cruz, F.W., Cheng, H., Karmann, I., Edwards, R.L., Vuille, M., Wang, X., de Paula, M.S., Novello, V.F., Auler, A.S., 2011. Abrupt variations in South American monsoon rainfall during the Holocene based on a speleothem record from central-eastern Brazil. Geology 39, 1075–1078.

Stuiver, M., Grootes, P.M., Braziunas, T.F., 1995. The GISP2 δ^{18}O climate record of the past 16,500 years and the role of the Sun, ocean and volcanoes. Quat. Res. 44, 341–354.

Thamban, M., Kawahata, H., Rao, V.P., 2007. Indian summer monsoon variability during the Holocene as recorded in sediments of the Arabian Sea: timing and implications. J. Oceanogr. 63, 1009–1020.

Thompson, L.G., Mosley-Thompson, E., Davis, M.E., Lin, P.-N., Henderson, K.A., Cole-Dai, J., Bolzan, J.F., Liu, K.-B., 1995. Late glacial stage and Holocene tropical ice core records from Huascaran, Peru. Science 269, 46–50.

Thompson, L.G., Davis, M.E., Mosley-Thompson, E., Sowers, T.A., Henderson, K.A., Zagorodnov, V.S., Lin, P.-N., Mikhalenko, V.N., Campen, R.K., Bolzan, J.F., Cole-Dai, J., Francou, B., 1998. A 25,000-year tropical climate history from Bolivian ice cores. Science 282, 1858–1864.

Thornalley, D.J.R., Elderfield, H., McCave, I.N., 2009. Holocene oscillations in temperature and salinity of the subpolar North Atlantic. Nature 457, 711–714.

Tobias, S.M., Weiss, N.O., 2000. Resonant interactions between solar activity and climate. J. Clim. 13, 3745–3759.

Torrence, C., Compo, G., 1998. A practical guide to wavelet analysis. Bull. Am. Meteorol. Soc. 79, 61–78.

Torrence, C., Webster, P., 1999. Interdecadal changes in ENSO-Monsoon system. J. Clim. 12, 2679–2690.

Traversi, R., Usoskin, I.G., Solanki, S.K., Becagli, S., Frezzotti, M., Severi, M., Stenni, B., Udisti, R., 2012. Nitrate in polar ice: a new tracer of solar variability. Sol. Phys. 280, 237–254.

Turney, C., Baillie, M., Clemens, S., Brown, D., Palmer, J., Pilcher, J., Reimer, P., Leuschner, H. H., 2005. Testing solar forcing of pervasive Holocene climate cycles. J. Quat. Sci. 20, 511–518.

Usoskin, I.G., 2013. A history of solar activity over millennia. Living Rev. Sol. Phys. 10, 1 (updated March 21, 2013; available at http://www.livingreviews.org/lrsp-2013-1).

Usoskin, I.G., Kromer, B., 2005. Reconstruction of the ^{14}C production rate from measured relative abundance. Radiocarbon 47, 31–37.

Usoskin, I.G., Alanko-Huotari, K., Kovaltsov, G.A., Mursula, K., 2005. Heliospheric modulation of cosmic rays: monthly reconstruction for 1951–2004. J. Geophys. Res. 110. http://dx.doi.org/10.1029/2005JA011250.

Usoskin, I.G., Solanki, S.K., Kovaltsov, G.A., 2007. Grand minima and maxima of solar activity: new observational constraints. Astron. Astrophys. 471, 301–309.

van Loon, H., Brown, J., Milliff, R.F., 2012. Trends in sunspots and North Atlantic sea-level pressure. J. Geophys. Res. 117. http://dx.doi.org/10.1029/2012JD017502.

Vasiliev, S.S., Dergachev, V.A., 2002. The 2400-year cycle in atmospheric radiocarbon concentration: bispectrum of 14C data over the last 8000 years. Ann. Geophys. 20, 115–120.

Velasco Herrera, V.M., 2013. The (super)-secular periodicity of the cosmic rays during the Holocene. In: Perez-Peraza, Jorge A. (Ed.), *Homage to the Discovery of Cosmic Rays, the Meson-Muon and Solar Cosmic Rays*, Nova, pp. 469–476 (chapter 15).

Vonmoos, M., Beer, J., Muscheler, R., 2006. Large variations in Holocene solar activity: constraints from ^{10}Be in the Greenland Ice Core Project ice core. J. Geophys. Res. 111. http://dx.doi.org/10.1029/2005JA011500.

Wang, Y.J., Cheng, H., Edwards, R.L., He, Y., Kong, X., An, Z.S., Wu, J., Kelly, M.J., Dykoski, C. A., Li, X., 2005. The Holocene Asian monsoon: links to solar changes and North Atlantic climate. Science 308, 854–857.

Wang, Y., Li, S., Luo, D., 2009. Seasonal response of Asian monsoonal climate to the Atlantic Multidecadal Oscillation. J. Geophys. Res. 114. http://dx.doi.org/10.1029/2008JD010929.

Wanner, H., Beer, J., Butikofer, J., Crowley, T.J., Cubasch, U., Fluckiger, Goosse, H., Grosjean, M., Joos, F., Kaplan, J.O., Kuttel, M., Muller, S.A., Prentice, I.C., Solomina, O., Stocker, T.F., Tarasov, P., Wagner, M., Widmann, M., 2008. Mid- to Late Holocene climate change: an overview. Quat. Sci. Rev. 27, 1791–1828.

Weiss, N.O., 2011. Solar and stellar dynamos. In: Brummell, N.H., Brun, A.S., Miesch, M.S., Ponty, Y. (Eds.), Astrophysical Dynamics: From Stars to Galaxies. Proceedings of the International Astronomical Union, IAU symposium, vol. 271, pp. 247–260.

Weng, H., 2012a. Impact of multi-scale solar activity on climate. Part I: Atmospheric circulation patterns and climate extremes. Adv. Atmos. Sci. 29, 867–886.

Weng, H., 2012b. Impact of multi-scale solar activity on climate. Part II: Dominant time-scales in decadal-centennial climate variability. Adv. Atmos. Sci. 29, 887–908.

Wiener, N., 1930. Generalized harmonic analysis. Acta Math. 55, 117–258.

Wilkins, D., Gouramanis, C., deDeckker, P., Fifield, L.K., Olley, J., 2013. Holocene lake-level fluctuations in Lakes Keilambete and Gnotuk, southwestern Victoria, Australia. The Holocene 23, 784–795. http://dx.doi.org/10.1177/0959683612471983.

Wolff, E.W., Bigler, M., Curran, M.A.J., Dibb, J.E., Frey, M.M., Legrand, M., McConnell, J.R., 2012. The Carrington event not observed in most ice core nitrate records. Geophys. Res. Lett. 39. http://dx.doi.org/10.1029/2012GL051603.

Wunsch, C., 2000. On sharp spectral lines in the climate record and the millennial peak. Paleoceanography 15, 417–424. http://dx.doi.org/10.1029/1999PA000468.

Xie, P., Vallis, G.K., 2012. The passive and active nature of ocean heat uptake in idealized climate change experiments. Clim. Dyn. 38, 667–684.

Yu, Y., Yang, T., Li, J., Liu, J., An, C., Liu, X., Fan, Z., Lu, Z., Li, Y., Su, X., 2006. Millennial-scale Holocene climate variability in the NW China drylands and links to the tropical Pacific and the North Atlantic. Palaeogeogr. Palaeoclimatol. Palaeoecol. 233, 149–162.

Zhao, C., Yu, Z., Ito, E., Zhao, Y., 2010. Holocene climate trend, variability, and shift documented by lacustrine stable-isotope record in northeastern United States. Quat. Sci. Rev. 29, 1831–1843.

Zhao, C., Liu, Z., Rohling, E., Yu, Z., Liu, W., He, Y., Zhao, Y., Chen, F., 2013. Holocene temperature fluctuations in the northern Tibetan Plateau. Quat. Res. 80, 55–65.